[AMERICAN JOURNAL OF SCIENCE, VOL. 288, OCTOBER, 1988, P. 827–871]

A GEOCHEMICAL STUDY OF ZONED INCLUSIONS IN GRANITIC ROCKS

J. J. CRAMER* and T. A. P. KWAK**

ABSTRACT. Six selected zoned enclaves found within four granitic plutons in southern Victoria, Australia were analyzed to determine the nature and cause of the zonation. Enclaves identified as restitic, autolithic, and xenolithic were analyzed having a wide range of compositions including calcic and peraluminous compositions. Bulk chemical analyses of the various zones present and the granitic rocks at the margins of the enclaves as well as of the constituent minerals were done to test whether the zonations observed can be explained by melt + restite mixing or by diffusional processes. Bulk chemical variations shown on CaO–Na_2O–K_2O ternary diagrams indicate non-linear (curved line) relationships for all six enclaves, whereas on SiO_2–TiO_2–Al_2O_3 diagrams (oxides of highly charged cations) a close approximation to linearity occurs. Using a TiO_2-fixed frame for the core of the enclaves as a reference, the oxides Al_2O_3, Na_2O, and usually K_2O can be shown to have been introduced to the reaction rim. The concentration patterns of other oxides, particularly SiO_2, FeO, MgO, and CaO, are highly variable.

Both the mineralogical and chemical data suggest the formation and composition of a reaction rim resulting from diffusion controlled mass transfer across the inclusion-magma interface. The driving force necessary for this transfer is the chemical potential difference seen by the mineralogical and compositional differences between the core and the magma.

INTRODUCTION

The origin of inclusions or "enclaves" within granitic intrusions is poorly understood partly because detailed bulk and mineral chemical analyses are rarely available. The main types of enclaves occur in granitic plutons as follows:

1. Material derived from the site of magma genesis representing material that did not melt (= "restite," for example Bateman and others, 1963; White and Chappell, 1977).
2. Material derived from within the granitoid magma. This probably represents the disruption of early differentiates of the magma (= microgranitoid enclaves, Vernon, 1983: cognate enclaves, Grout, 1937; or autolith, Pabst, 1928).
3. Material derived from the wall rocks and accidentally incorporated in the magma (= xenolith enclaves).

Enclaves exhibiting zonation are relatively common (for example, Reynolds, 1946; Didier, 1973; Vernon, 1983). They are probably the most useful to determine the origin of enclaves, because the processes that have altered or produced them were arrested before completion.

* Atomic Energy of Canada, Whiteshed Nuclear Research Establishment, Pinawa, Manitoba ROE 1LO Canada.

** Department of Geology, La Trobe University, Bundoora, Victoria, Australia 3083

Zoned enclaves may have either well defined zones with visually sharp boundaries, each zone being internally more-or-less homogeneous, or gradational changes exist in part of the enclave where the mineralogical and/or bulk composition changes gradationally. Particularly in the latter case, individual zones based on mineralogical and color changes are commonly concentric around a central core.

There have been many criteria used to distinguish between the three enclave types summarized by White and Chappell (1977), Hine and others (1978), Griffin, White, and Chappell (1978), and more recently by Vernon (1983). Field, microstructural, petrographic, and chemical data, some of which may be conflicting, are used. The evidence is too numerous to discuss here but generally involves identifying relict features as opposed to later overprinted effects as summarized by Vernon (1983).

The purpose of this study is (1) to document bulk chemical changes in various zones in the enclaves and see how these differ compared to the host pluton, (2) document mineral chemical and mineral species changes in various zones, and (3) suggest an origin for the zoned enclaves.

GEOLOGICAL SETTING AND SAMPLE SELECTION

The zoned enclaves for which data are presented here have been taken from four granitoids located in central Victoria, Australia. These are the Tynong and Bulla Adamellites and the Lysterfield and Warbuton Granodiorites. All four plutons are high level intrusions having sharp contacts with the country rocks and well developed contact metamorphic aureoles. The granite in and around each of the localities, from which the enclaves were sampled, is massive and non-foliated: no noticeable orientation of the enclaves was observed. Data on the geology and chemistry of the Tynong, Lysterfield, and Warbuton plutons are given by Cramer (ms) and of the Bulla Adamellite by Bryndzia (ms).

In all four plutons the abundance of zoned enclaves is low compared to non-zoned, apparently homogeneous enclaves. The total abundance of inclusions varies locally, but, in general, the concentration of enclaves is highest near the outer edges of the plutons. Bryndzia (ms) found that amphibole-bearing enclaves are the only zoned types in the Bulla Adamellite; they make up about 7 percent of all inclusions. The abundance of enclaves in the Tynong Adamellite is very low, and zoned inclusions are rare. In the Warbuton and Lysterfield Granodiorites, enclaves contribute about 2 and 5 volume percent, respectively. Few zoned enclaves occur in the Warbuton pluton, and the one selected for study is the only one that is amphibole-bearing. In the Lysterfield Granodiorite, zoned enclaves make up about 5 percent of all enclaves.

On the basis of studies of large numbers of enclaves in all four plutons, six zoned enclaves were selected for detailed study. These are believed to represent restite, autolithic, and xenolithic materials. Although the number of samples studied is relatively small, the variety of mineral assemblages in both the host plutons and the inclusions

covers most of the possible range of chemical and physical variations present in granite environments. The minerals present in the enclaves include clinopyroxene, clino-amphibole, ortho-amphibole, cordierite, and garnet. The characteristic assemblages in the granites, however, include clinoamphibole + biotite, biotite alone, and cordierite + biotite. Brief descriptions for each of the selected inclusions and their host granite are given in app. 1, and they are shown in figures 1 to 6 which also show the parts of the enclaves selected for bulk rock and mineral analyses.

CHEMISTRY

For each of the zoned enclaves, whole rock and mineral chemical compositions have been determined along a continuous profile across the enclave and into the host granite, as illustrated in figure 1A to F. For most of the whole rock samples, 10 to 15 cm^3 of rock were used for analysis. For the granites and the larger cores of enclaves (B), (C), and (F), the analytical sample volume was approx 250 cm^3. Polished thin sections used for mineral analyses were taken from the same sample chips used for bulk rock analysis. The bulk rock analyses for inclusion (B) are from Bryndzia (ms). Modal analyses were performed by point counting (min 1500 points) on thin sections. The analytical data for the whole rock samples are given in table 1 whereas the analytical data for the analyzed minerals are given in table 2.

The whole rock compositions in table 1 show generally that all inclusions have lower FeO_t/FeO_t + MgO ratios (Fe-factors) for the cores, compared with their host granite. All enclaves except (D) have lower SiO_2 and higher CaO-contents, and all enclaves except (A) have higher Al_2O_3 contents for the core relative to the granite. Similarly, for enclaves (A), (B), (C), and (D), the cores have lower Na_2O and K_2O-contents, whereas for enclaves (E) and (F), the Na_2O-contents are higher, and the K_2O-contents are lower for the cores.

Variations in the compositions of the mafic minerals, in particular of biotite and amphibole (table 2), generally follow the bulk rock trends. The changes in biotite and amphibole composition are most distinct for those enclaves for which the Fe-factors of the core and of the granite differ most (enclaves B and D) and for those that have peraluminous compositions for both enclave and granite (inclusions B and C).

Material balance relations.—To illustrate the processes involved in generating the reaction zones of the inclusions, variation diagrams are used. In the case of mechanical mixing, bulk rock compositions plotted, for example, on an AFM diagram will lie on a linear trend that intersects a mineral stability field irrespective of the compositions of that mineral. On the other hand, selective mass transfer by diffusion as well as an origin by fractional crystallization will result in bulk rock trends that are related to changes in the relevant mineral compositions, and the trends will generally be curved. If the composition of a suite of related rocks results from purely mechanical mixing of only two endmembers of fixed

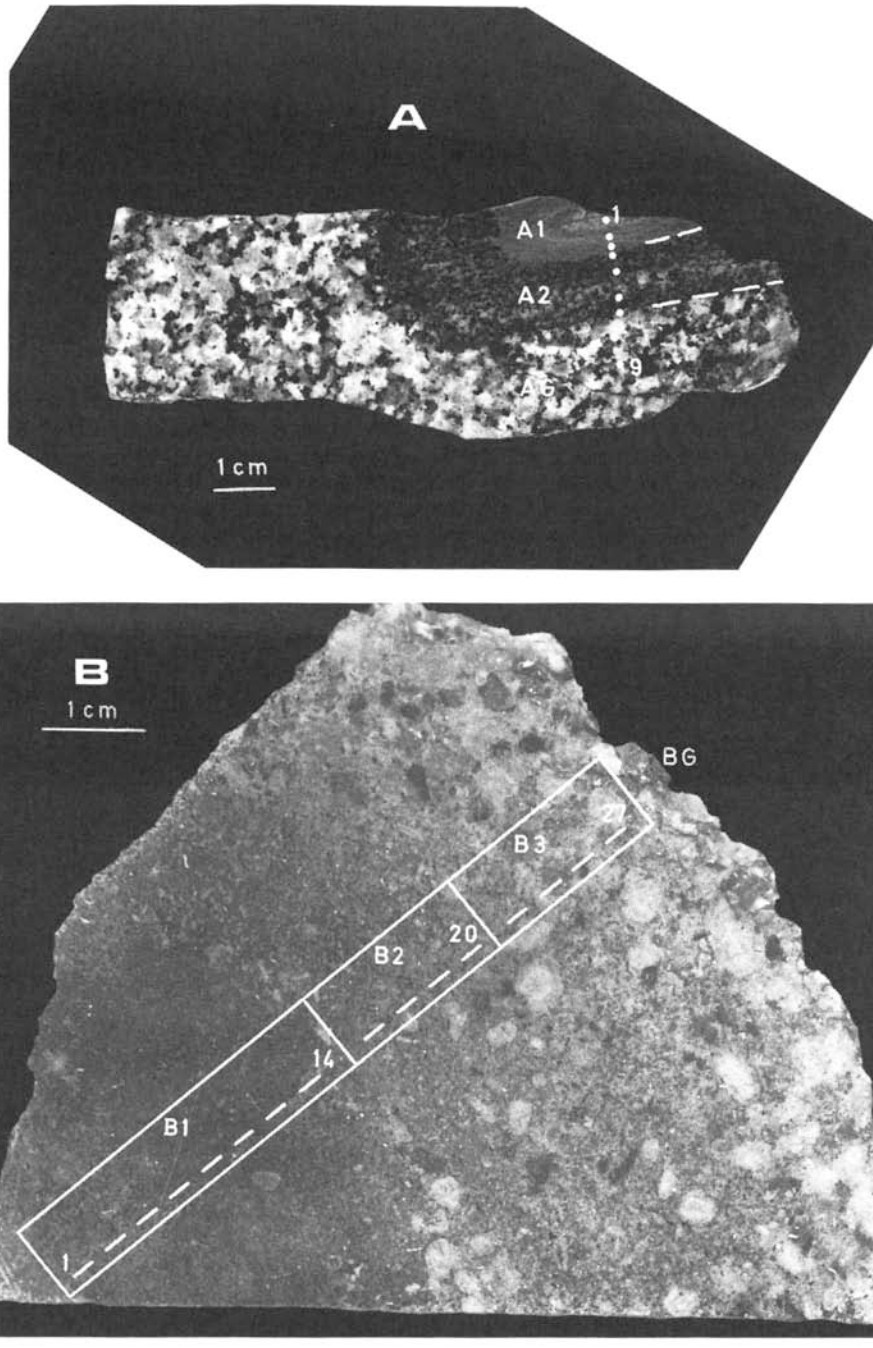

Fig. 1(A) Cross section of enclave (A) showing whole rock sample profile (A1-2,AG) and sample locations (1–9) for mineral analyses.

(B) Cross section of enclave (B) showing whole rock sample profile (B1-3,BG) and sample locations (1–27) for mineral analyses.

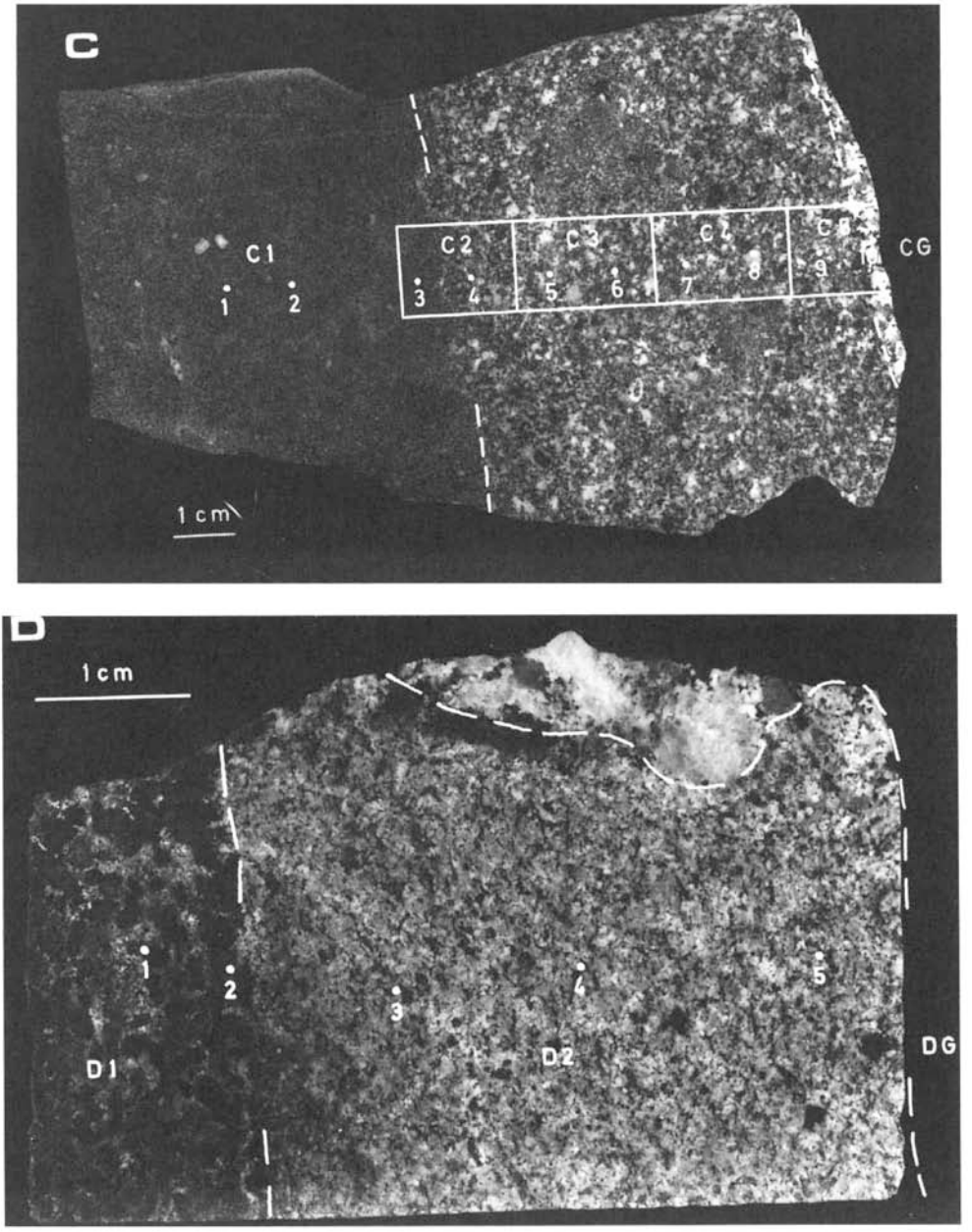

Fig. 1. (continued)
(C) Cross section of enclave (C) showing whole rock sample profile (C1-5,CG) and sample locations (1–10) for mineral analyses.
(D) Cross section of enclave (D) showing whole rock sample profile (D1-2,DG) and sample locations (1–5) for mineral analyses.

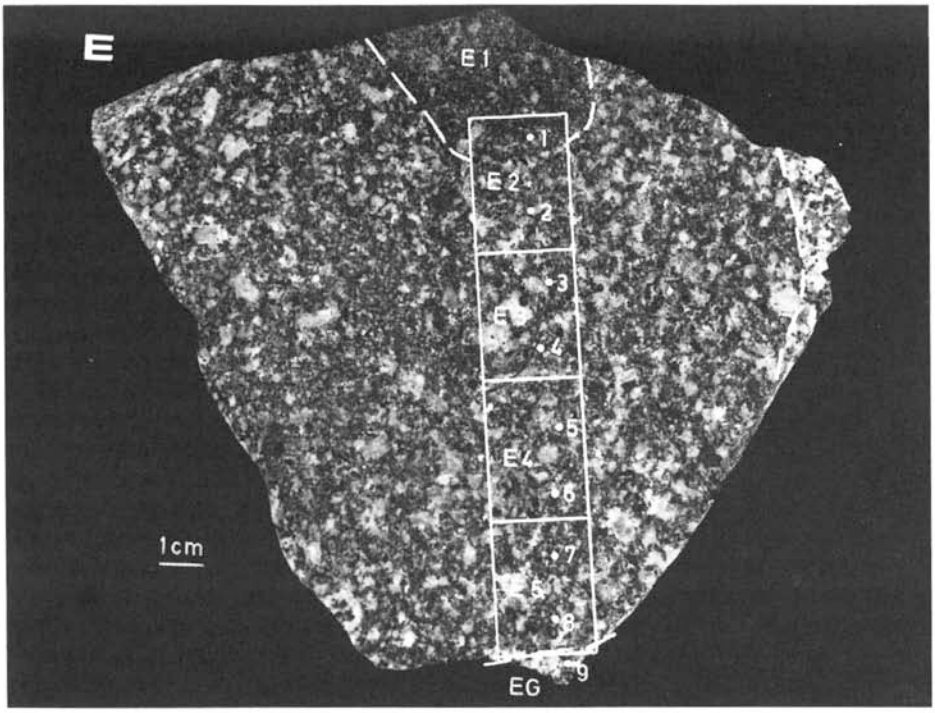

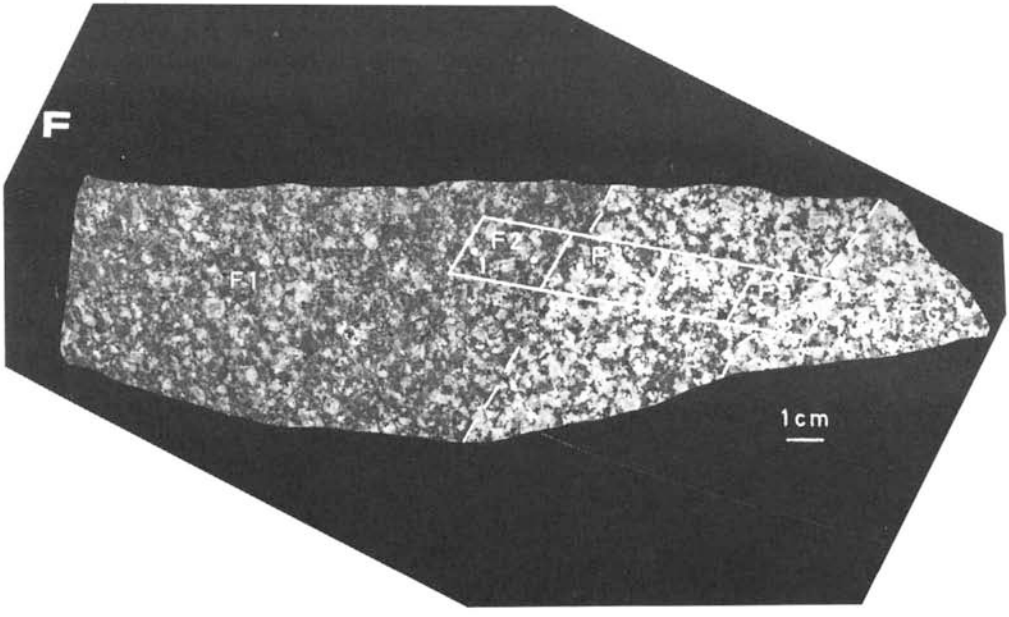

Fig. 1. (continued)

(E) Cross section of enclave (E) showing whole rock sample profile (E1-5,EG) and sample locations (1–9) for mineral analyses.

(F) Cross section of enclave (F) showing whole rock sample profile (F1-5,FG) and sample locations (1–8) for mineral analyses.

compositions then bulk rock trends will be linear. This may not be the case if more than two endmember compositions are mixed. Alternatively, in the case of diffusional processes, curved bulk rock trends are most common, although for some, near-linear trends may still occur.

In figure 2 bulk rock major element data for each of the inclusions are plotted on two different diagrams: one for the (lower charged = L.I.L.) alkali species (NA^+, K^+ and $Ca2^+$) and one for the highly charged (H.C.C.) species (AL^{3+}, $Si4^+$ and Ti^{4+}). The bulk rock trends are distinctly non-linear on the CaO–Na_2O–K_2O diagrams. On the SiO_2–TiO_2–Al_2O_3 diagrams the trends appear more linear, but, in detail, the compositions of the reaction zone of each inclusion deviate from a straight line. Also the AFM diagrams in figures 3 to 8 show similar characteristics for the bulk rock trends, which in some cases are clearly related to distinct mineral composition trends. It is evident from these diagrams that diffusion must have contributed significantly to the formation of the reaction zone in each of these enclaves, implying an autolithic or xenolithic origin is unlikely.

To evaluate mass transfer by diffusion an appropriate reference frame is required. Upon formation of a reaction zone by diffusion, changes in the composition of both inclusion and granite result from transport along chemical potential gradients. As a result, not all elements will necessarily take part in the mass transfer. Compositions may change with respect to all elements by introduction or removal of the diffusing species. It is therefore necessary to choose a fixed parameter in the system to which the chemical changes can be referred (Brady, 1975). This fixed parameter or reference frame can be the initial boundary between inclusion and granite, a volume-fixed frame, or a component-fixed frame (for example, Thompson, 1957). For a system that contains a solid and a liquid phase, initial boundaries in the crystalline rock may be difficult to recognize; particularly when a reaction zone has formed. It can be argued that this is more likely in the case of a restite enclave which itself probably consists of a solid + melt, as opposed to a xenolith which may not contain any melt. Hence, the use of an initial boundary as a reference is difficult to justify. A volume-fixed frame can be applied only if there is good evidence for the original composition of the enclave.

Mass transfer is discussed here using a TiO_2-fixed reference frame. The composition for the core of the inclusion is chosen as the reference. In a component-fixed frame the flux (a measure for the 'mobility') of all other components is related to that of the reference component. This does not mean that the selected component is necessarily immobile, but it is considered to have the smallest flux compared to the other components. Al, Ti, Zr, and Cr are commonly suggested as suitable 'least mobile' elements in various geological processes (for example, Carmichael, 1969; Thompson, 1957). This is based mainly on evidence from the ceramic literature concerning the diffusion kinetics in silicate

TABLE 1

Major and trace element analyses of whole rock samples and modes for enclaves (A) to (F). For sample numbers see figure 1A to F

INCLUSION	(A)			(B)				(C)					
SAMPLE	A1	A2	AF-FG	B1	B2	B3	BG	C1	C2	C3	C4	C5	CG
wt. %													
SiO_2	58.14	60.80	67.34	60.65	61.28	66.73	69.02	60.11	63.50	61.93	64.57	65.65	67.57
TiO_2	0.62	0.66	0.61	1.42	1.37	0.92	0.58	1.06	0.96	0.94	0.83	0.79	0.65
Al_2O_3	12.87	13.72	14.71	15.83	15.63	15.12	14.94	16.09	15.52	15.40	15.02	14.90	14.52
Fe_2O_3	0.06	0.77	0.33	1.15	1.06	0.79	0.37	0.58	0.42	0.54	0.30	0.21	0.15
FeO	5.05	5.73	3.32	6.59	6.47	4.58	3.11	5.99	5.18	5.26	4.72	4.38	3.63
MnO	0.32	0.18	0.07	0.12	0.11	0.07	0.05	0.12	0.09	0.09	0.08	0.08	0.06
MgO	3.49	4.30	2.17	3.43	3.20	1.80	1.20	4.22	3.26	3.29	2.83	2.59	2.28
CaO	15.12	6.54	3.64	4.91	3.92	2.89	2.35	5.55	4.57	4.11	4.02	3.58	2.61
Na_2O	2.07	4.10	3.59	1.08	1.78	3.15	2.89	1.53	2.29	2.46	2.59	2.55	2.35
K_2O	0.10	0.95	2.98	2.16	2.66	2.21	3.76	2.59	2.56	2.87	2.41	3.09	6.50
P_2O_5	0.14	0.17	0.10	0.20	0.23	0.21	0.15	0.21	0.18	0.18	0.16	0.16	0.12
S	0	0	0.01	0	0	0	0	0.07	0.08	0.06	0.06	0.06	0.06
H_2O^+	0.42	0.91	0.75	1.75	1.60	1.14	1.10	1.47	1.20	1.56	1.25	1.20	0.93
H_2O^-	0.20	0.07	0.04	0.41	0.27	0.37	0.11	0.20	0.07	0.02	0.10	0.10	0.14
CO_2	0.93	0.20	0.06	0.17	0.27	0.18	0.40	0.26	0.33	0.33	0.41	0.29	0.59
-S = 0	0	0	0	0	0	0	0	0.03	0.04	0.03	0.03	0.03	0.03
TOTAL	99.53	99.10	99.72	99.87	99.85	100.16	100.03	100.02	100.17	99.01	99.32	99.60	100.13
Al-Factor	-1.165	-0.289	-0.081	0.185	0.192	0.257	0.307	0.064	0.074	0.079	0.093	0.103	0.129
Fe-Factor	0.422	0.432	0.442	0.509	0.521	0.582	0.577	0.425	0.447	0.455	0.457	0.455	0.439
Spec. gravity	3.042	2.886	2.729	2.897	2.741	3.659	2.691	2.808	2.786	2.763	2.751	2.728	2.714
ppm													
Ba	44	174	705	-	-	-	-	965	908	806	716	984	1335
Rb	5	42	137	-	-	-	-	140	165	214	186	194	210
Sr	222	163	331	-	-	-	-	308	322	271	263	256	248
Pb	12	24	27	-	-	-	-	18	16	22	20	24	34
Th	44	9	19	-	-	-	-	16	12	16	16	17	20
U	7	3	3	-	-	-	-	4	1	2	2	4	5
Zr	172	197	178	-	-	-	-	186	195	248	260	254	246
Nb	12	21	16	-	-	-	-	19	17	18	18	19	16
Y	39	69	21	-	-	-	-	48	27	32	29	34	38
La	47	26	30	-	-	-	-	37	30	33	37	35	35
Ce	95	76	61	-	-	-	-	79	67	67	68	70	77
V	88	135	79	-	-	-	-	183	155	155	129	112	84
Cr	105	120	55	-	-	-	-	56	78	84	85	89	78
Ni	86	97	59	24	26	23	19	63	62	68	71	66	65
Cu	67	27	69	41	35	24	25	51	54	43	43	48	41
Zn	76	79	43	107	133	114	66	80	77	86	76	68	56
Ga	17	18	18	-	-	-	-	20	20	21	21	19	17
vol %													
Diopside	41.7	0.6	0										
Amphibole	0	32.0	7.2	12.1	1.7	0	0	6.6	1.4	0.1	0	0	0
Biotite	0	1.7	11.0	22.2	32.5	28.8	23.0	23.4	27.0	21.2	20.4	20.1	19.5
Carbonate	13.2	0	0										
Sphene	0.06	0.08	0.13										
Opaque	0.03	0.05	0.03	2.17	0.90	0.80	0.21	0.26	0.38	0.27	0.19	0.16	0.12
Garnet				0	0	0.9	0						
Cordierite				0	0	0.6	3.2						

TABLE 1
(Continued)

INCLUSION		(D)					(E)					(F)		
SAMPLE	D1	D2	DG	E1	E2	E3	E4	E5	EG	F1	F2	F3	F4	F5
wt. %														
SiO_2	79.21	67.34	71.44	58.53	62.87	62.12	61.59	63.85	66.05	57.53	57.04	64.21	64.36	65.27
TiO_2	0.36	0.41	0.40	1.15	0.80	0.85	0.83	0.79	0.67	0.99	1.03	0.78	0.78	0.78
Al_2O_3	5.47	15.67	14.39	15.29	14.92	14.61	14.79	14.36	14.65	15.12	15.09	14.88	15.23	14.53
Fe_2O_3	0.80	0.35	0.12	1.96	1.28	1.33	1.21	1.10	1.03	1.26	1.12	0.69	0.69	0.63
FeO	4.75	2.80	2.41	5.38	4.20	4.56	4.64	4.35	3.05	5.91	6.37	4.27	4.01	4.03
MnO	0.14	0.06	0.05	0.14	0.11	0.12	0.12	0.11	0.07	0.15	0.16	0.09	0.09	0.08
MgO	2.88	1.24	0.91	4.29	3.35	3.62	3.59	3.36	2.23	4.62	4.77	3.11	2.77	2.64
CaO	2.34	3.76	2.38	4.71	4.09	5.00	5.08	4.17	3.76	6.42	6.41	4.86	4.64	4.17
Na_2O	0.79	4.59	3.77	3.72	3.71	3.61	3.69	3.68	3.49	3.69	3.64	3.80	3.89	3.63
K_2O	2.85	1.87	3.49	2.90	2.02	2.15	2.17	1.81	3.07	1.93	1.99	1.82	1.96	2.39
P_2O_5	0.09	0.09	0.04	0.18	0.14	0.15	0.15	0.13	0.09	0.19	0.21	0.14	0.13	0.13
S	0.09	0.01	0.02	-	0	0	0	0	-	-	0.01	0	0	0
H_2O^+	0.74	0.67	0.70	1.18	0.99	1.05	1.11	1.00	0.80	1.21	1.18	0.84	0.80	0.84
H_2O^-	0.09	0.16	0.15	0.13	0.08	0.10	0.03	0.11	0.16	0.12	0.04	0.05	0.07	0.10
CO_2	0.17	0.04	0.08	0.09	0.15	0.14	0.19	0.18	0.08	0.47	0.26	0.19	0.22	0.16
-S=0	0.02	0	0.01	-	0	0	0	0	-	-	0.10	0	0	0
TOTAL	100.70	99.06	100.34	99.65	99.71	99.41	99.19	99.65	99.20	99.61	99.31	99.73	99.64	99.38
Al-Factor	-0.207	-0.075	0.033	-0.108	-0.152	-0.147	-0.155	-0.136	-0.099	-0.209	-0.198	-0.133	-0.113	-0.106
Fe-Factor	0.501	0.554	0.571	0.444	0.437	0.436	0.438	0.436	0.459	0.428	0.431	0.430	0.443	0.453
Spec. gravity	2.766	2.696	2.668	2.837	2.792	2.775	2.777	2.759	2.725	2.846	2.842	2.770	2.767	2.755
ppm														
Ba	640	321	1167	663	502	518	511	437	819	517	547	514	562	559
Rb	150	145	158	206	139	147	142	137	148	68	133	121	131	143
Sr	46	183	183	272	341	312	300	315	382	328	319	354	370	325
Pb	18	24	24	22	20	20	21	20	26	21	20	20	20	21
Th	10	8	31	7	7	6	7	9	19	4	7	6	7	14
U	2	4	5	10	10	9	9	7	4	30	8	5	5	4
Zr	198	125	231	141	360	406	335	169	187	231	259	220	233	223
Nb	13	17	16	29	24	26	25	24	17	23	26	19	20	21
Y	81	29	37	34	37	38	41	35	22	65	54	29	26	24
La	28	15	54	13	18	16	18	18	38	23	21	15	14	18
Ce	75	33	100	44	51	46	50	42	69	67	68	40	41	45
V	76	40	34	154	121	128	127	116	89	158	168	111	104	101
Cr	34	8	17	136	107	113	119	103	58	197	210	101	73	76
Ni	51	20	18	103	112	131	133	112	69	212	221	107	53	57
Cu	638	41	21	166	77	72	94	68	65	435	448	343	343	192
Zn	124	54	46	93	69	72	71	65	50	93	102	63	61	60
Ga	8	19	18	20	21	19	19	19	18	22	21	19	20	19
vol %														
Amphibole	20.3	3.3	1.1	14.8	12.5	16.3	13.2	12.8	5.2	28.2	29.4	13.1	8.9	6.5
Biotite	8.1	7.6	6.7	20.9	17.9	14.0	13.8	13.4	10.2	17.4	16.0	13.7	13.3	14.0
Sphene				0.33	0.40	0.33	0.20	0.26	0.09	0.10	0.26	0.06	0.06	0.07
Opaque	0.39	0.08	0.19	0.03	0.05	0.03	0.03	0.02	0.04	0.02	0.03	0.02	0.02	0.01

TABLE 2

Electron microprobe analyses of characteristic ferromagnesian silicates from inclusions (A) to (F). Sample numbers for the minerals correspond to locations in figure 1A to F

INCLUSION (A)

	PYROXENE						AMPHIBOLE			
	A1 1	A1 2	A1 3	A1 4	A1 4	A1 4a	A2 5	A2 6	A2 7	AG 8
SiO_2	50.79	50.22	51.90	51.60	47.77	47.05	46.63	47.89	51.65	46.02
TiO_2	0.03	0.12	0.26	0.11	0.99	1.25	1.27	1.10	0.61	1.39
Al_2O_3	0.59	0.94	0.63	0.72	5.91	6.13	6.51	5.55	2.68	6.77
FeO_t	12.09	13.11	11.44	10.51	15.85	15.73	16.75	16.14	15.14	16.86
MnO	0.80	0.73	0.54	0.69	0.48	0.34	0.41	0.45	0.52	0.52
MgO	8.74	8.52	10.44	11.64	11.15	11.15	11.10	11.86	13.13	10.38
CaO	24.23	24.37	23.43	22.26	11.72	11.72	11.30	11.26	11.68	11.69
Na_2O	0.13	0.16	0.29	0.31	1.04	1.23	1.31	1.13	0.56	1.31
K_2O	0.02	0	0.02	0	0.57	0.62	0.57	0.50	0.23	0.62
P_2O_5	0.01	0.01	0	0.03	0.04	0.06	0.05	0.01	0.03	0.06
F	0.02	0	0	0.01	0	0.25	0.13	0.01	0.26	0.21
Cl	0.01	0	0.01	0.02	0.02	0.03	0.04	0.02	0.02	0.03
-F, Cl=0	0.02	0	0	0.01	0	0.11	0.06	0.01	0.11	0.09
TOTAL	97.44	98.18	98.96	97.89	95.54	95.45	96.11	95.91	96.40	95.77
Al-Factor	-1.113	-1.090	-1.004	-0.909	-0.357	-0.362	-0.332	-0.336	-0.365	-0.355
Fe-Factor	0.436	0.461	0.367	0.334	0.429	0.424	0.441	0.418	0.384	0.458

	AMPHIBOLE						BIOTITE		
	AG 9	AG	A2 4	A2 5	A2 6	A2 7	AG 8	AG 9	AG
SiO_2	46.36	46.94	36.21	36.40	36.09	36.52	36.43	35.69	35.43
TiO_2	1.26	1.30	4.67	4.54	4.99	4.64	5.23	4.86	4.56
Al_2O_3	6.61	6.21	13.55	13.57	13.29	13.17	13.61	13.51	13.52
FeO_t	16.25	16.18	19.96	19.02	20.20	19.89	19.97	19.81	21.19
MnO	0.45	0.52	0.21	0.25	0.21	0.26	0.23	0.21	0.35
MgO	11.88	11.85	9.91	10.46	10.02	10.24	9.89	10.39	10.53
CaO	11.70	11.23	0.03	0.01	0	0	0	0	0
Na_2O	1.30	1.29	0.07	0.08	0.12	0.08	0.13	0.14	0.09
K_2O	0.56	0.44	9.89	9.91	9.72	0.82	9.63	9.52	9.36
P_2O_5	0.04	0.04	0.01	0.03	0.02	0.02	0.04	0.02	0.01
F	0.11	0.17	0.15	0.29	0.23	0.20	0.32	0.28	0.38
Cl	0.02	0.05	0.06	0.04	0.05	0.04	0.07	0.05	0.04
-F, Cl=0	0.05	0.07	0.07	0.13	0.11	0.09	0.15	0.13	0.17
TOTAL	96.49	96.15	94.65	94.47	94.83	94.79	95.40	94.35	95.29
Al-Factor	-0.336	-0.326	0.057	0.058	0.054	0.050	0.064	0.062	0.064
Fe-Factor	0.417	0.415	0.472	0.445	0.468	0.462	0.464	0.455	0.477

TABLE 2
(Continued)

INCLUSION (B)

	AMPHIBOLE				BIOTITE					
	B1 1	B1 5	B1 9	B1 13	B1 1	B1 2	B1 3	B1 4	B1 5	B1 6
SiO_2	53.53	46.76	50.81	49.52	35.96	36.02	35.76	35.91	36.14	38.28
TiO_2	0.10	0.21	0.14	0.88	3.62	3.00	3.43	3.06	3.26	3.20
Al_2O_3	1.29	4.31	4.83	8.50	14.89	14.84	14.83	14.65	14.47	14.64
FeO_t	28.88	29.77	26.16	25.84	20.99	20.56	20.79	21.45	21.00	20.31
MnO	0.88	0.99	0.93	0.96	0.17	0.19	0.16	0.17	0.28	0.22
MgO	12.61	12.41	11.68	10.14	9.65	9.71	9.21	9.35	9.79	9.81
CaO	0.43	0.52	0.60	0.45	0.01	0.03	0.02	0	0	0.01
Na_2O	0.13	0.13	0.16	0.11	0.24	0.21	0.24	0.20	0.23	0.23
K_2O	0.01	0.52	0.46	0.48	9.04	8.90	8.91	9.18	9.10	9.06
P_2O_5	-	-	-	-	-	-	-	-	-	-
F	-	0.39	0.24	0.22	0.71	0.59	0.71	0.79	0.80	0.65
Cl	-	0.02	0.03	0.02	0.04	0.04	0.04	0.04	0.04	0.02
-F, Cl=0	-	0.17	0.11	0.10	0.31	0.26	0.31	0.34	0.34	0.24
TOTAL	97.86	95.86	95.93	97.02	95.01	93.83	93.79	94.46	94.77	96.19
Al-Factor	0.004	0.035	0.045	0.114	0.095	0.096	0.098	0.087	0.084	0.090
Fe-Factor	0.562	0.572	0.556	0.581	0.508	0.508	0.519	0.529	0.509	0.499

	BIOTITE									
	B1 7	B1 8	B1 9	B1 10	B1 11	B1 12	B1 13	B1 14	B2 15	B2 16
SiO_2	36.25	35.61	35.36	35.99	34.95	35.74	35.38	34.65	35.33	34.36
TiO_2	2.73	3.97	3.47	3.85	3.93	4.02	4.10	4.39	4.10	4.13
Al_2O_3	14.89	15.38	15.68	16.12	15.01	15.28	15.78	16.08	15.97	16.14
FeO_t	21.17	21.29	20.92	21.08	21.92	21.75	21.96	22.21	22.33	21.59
MnO	0.19	0.28	0.24	0.22	0.27	0.24	0.27	0.21	0.23	0.22
MgO	9.71	9.00	8.45	9.23	8.07	7.99	8.37	7.92	7.92	7.42
CaO	0	0.05	0.07	0.06	0.01	0	0.01	0	0	0
Na_2O	0.15	0.27	0.31	0.24	0.24	0.23	0.27	0.25	0.19	0.20
K_2O	9.15	9.24	8.78	9.15	9.20	9.42	9.40	9.46	9.41	9.51
P_2O_5	-	-	-	-	-	-	-	-	-	-
F	0.52	0.58	0.48	0.51	0.69	0.35	0.54	0.38	0.59	0.42
Cl	0.04	0.04	0.04	0.06	0.03	0.04	0.02	0.04	0.03	0.05
-F, Cl=0	0.23	0.26	0.11	0.23	0.30	0.16	0.23	0.17	0.26	0.19
TOTAL	94.57	95.45	93.69	95.28	94.02	94.90	95.87	95.42	95.84	93.85
Al-Factor	0.093	0.101	0.119	0.125	0.100	0.102	0.109	0.118	0.118	0.125
Fe-Factor	0.520	0.525	0.542	0.546	0.561	0.560	0.551	0.564	0.569	0.575

TABLE 2
(Continued)

	BIOTITE									
	B2 17	B2 18	B2 19	B2 20	B3 21	B3 22	B3 23	B3 24	B3 25	B3 26
SiO_2	35.19	34.25	34.72	33.77	34.36	34.29	34.88	34.62	34.56	34.28
TiO_2	3.89	4.15	4.12	4.24	4.21	4.09	4.32	4.21	4.04	4.35
Al_2O_3	16.08	16.43	16.57	16.62	16.77	16.75	16.36	16.41	16.55	16.23
FeO_t	21.33	22.00	22.14	22.09	22.27	21.78	22.26	21.86	21.96	22.14
MnO	0.22	0.24	0.22	0.24	0.23	0.28	0.28	0.22	0.21	0.29
MgO	7.47	7.39	7.23	7.15	7.32	7.13	7.41	7.22	7.16	7.01
CaO	0	0	0	0	0	0	0	0	0	0
Na_2O	0.20	0.21	0.19	0.19	0.16	0.20	0.20	0.19	0.17	0.21
K_2O	9.66	9.47	9.61	9.30	9.61	9.57	9.33	9.57	9.45	9.34
P_2O_5	-	-	-	-	-	-	-	-	-	-
F	0.32	0.40	0.43	0.34	0.54	9.43	0.44	0.57	0.52	0.40
Cl	0.06	0.06	0.04	0.06	0.05	0.05	0.07	0.04	0.05	0.07
-F, Cl=0	0.15	0.18	0.19	0.16	0.24	0.19	0.20	0.25	0.23	0.18
TOTAL	94.27	94.42	95.08	93.84	95.28	94.38	95.35	94.66	94.44	94.14
Al-Factor	0.120	0.131	0.132	0.142	0.136	0.139	0.132	0.131	0.137	0.132
Fe-Factor	0.573	0.581	0.589	0.589	0.586	0.588	0.582	0.584	0.590	0.593

	BIOTITE					GARNET			CORDIERITE	
	B3 27	BG 28	BG 29	BG 30	BG 31	B3 26	B3 26a	B3	B3 27	BG
SiO_2	35.14	35.01	34.83	34.61	35.04	36.43	35.69	35.42	48.83	47.93
TiO_2	4.35	4.02	4.07	4.39	4.30	0.05	0.02	0	0.01	0
Al_2O_3	16.45	16.74	17.01	16.54	16.94	20.60	21.32	20.85	32.75	32.65
FeO_t	22.03	22.41	22.42	22.46	22.33	33.38	34.23	34.78	8.99	9.78
MnO	0.23	0.29	0.28	0.22	0.23	2.59	3.01	4.89	0.21	0.35
MgO	7.08	7.32	7.00	7.03	7.14	4.13	4.08	2.96	7.38	6.96
CaO	0	0	0	0	0	1.21	1.26	0.24	0.01	0.02
Na_2O	0.18	0.22	0.17	0.17	0.24	0.02	0.04	0	0.30	0.33
K_2O	9.41	9.32	9.41	8.92	9.22	0.01	0	0.03	0.02	0.03
P_2O_5	-	-	-	-	-	-	-	-	-	-
F	0.53	0.43	0.31	0.33	0.45	0.08	0.02	-	-	-
Cl	0.03	0.08	0.09	0.10	0.11	0.01	0	-	-	-
-F, Cl=0	0.23	0.20	0.15	0.16	0.21	0.03	0.01	-	-	-
TOTAL	95.20	97.64	95.44	94.61	95.79	98.48	99.66	99.17	98.50	98.05
Al-Factor	0.137	0.139	0.148	0.150	0.148	0.299	0.300	0.319	1.026	1.018
Fe-Factor	0.589	0.590	0.601	0.596	0.592	0.770	0.768	0.773	0.406	0.441

TABLE 2
(Continued)
INCLUSION (C)

	AMPHIBOLE				BIOTITE			
	C1 1	C1 2	C1 2a	C2 3	C1 1	C1 2	C2 3	C2 4
SiO_2	52.44	52.40	54.76	52.71	36.04	36.27	35.95	35.05
TiO_2	0.09	0.09	0.11	0.15	3.74	3.89	3.21	3.90
Al_2O_3	1.09	1.65	0.82	0.49	13.96	13.89	14.29	14.65
FeO_t	20.24	22.27	23.61	24.82	18.30	18.67	18.70	19.10
MnO	1.14	0.78	0.77	0.82	0.10	0.12	0.23	0.15
MgO	14.84	15.08	15.15	14.40	11.20	11.03	11.54	10.78
CaO	5.39	3.36	2.46	1.25	0	0.02	0	0
Na_2O	0.12	0.17	0.10	0.06	0.13	0.16	0.13	0.15
K_2O	0.05	0.02	0.04	0.02	9.54	9.48	9.57	9.40
P_2O_5	0	0.06	0.03	0.01	0	0.06	0.01	0.04
F	0.09	0.16	0.12	0.11	0.28	0.41	0.27	0.29
Cl	0	0.01	0.02	0.03	0.10	0.09	0.03	0.05
-F, Cl=0	0.04	0.07	0.06	0.05	0.14	0.19	0.12	0.13
TOTAL	95.45	95.98	97.93	94.82	93.25	93.90	93.81	93.43
Al-Factor	-0.135	-0.066	-0.053	-0.026	0.069	0.070	0.072	0.086
Fe-Factor	0.433	0.452	0.465	0.490	0.428	0.436	0.435	0.448

	BIOTITE						
	C3	C3	C4	C4	C5	C5	CG
SiO_2	35.57	35.05	35.77	35.31	35.38	34.21	34.58
TiO_2	3.25	3.83	3.45	3.49	3.26	3.04	3.43
Al_2O_3	14.61	14.77	15.12	14.94	15.10	16.36	17.59
FeO_t	18.79	18.79	18.52	18.52	18.39	18.12	18.07
MnO	0.26	0.19	0.27	0.22	0.25	0.41	0.31
MgO	10.93	10.99	10.95	10.95	10.56	10.22	10.28
CaO	0.01	0.02	0	0	0	0	0
Na_2O	0.12	0.13	0.10	0.11	0.13	0.13	0.11
K_2O	9.53	9.62	9.41	9.58	9.67	9.29	9.33
P_2O_5	0	0	0.02	0	0	0	0
F	0.50	0.39	0.36	0.44	0.67	0.32	0.25
Cl	0.04	0.03	0.07	0.06	0.07	0.05	0.03
-F, Cl=0	0.22	0.17	0.16	0.20	0.30	0.14	0.11
TOTAL	93.39	93.64	93.88	93.42	93.18	92.01	93.89
Al-Factor	0.081	0.083	0.096	0.089	0.091	0.128	0.155
Fe-Factor	0.449	0.439	0.441	0.441	0.451	0.456	0.450

TABLE 2
(Continued)

INCLUSION (D)

	AMPHIBOLE					
	D1 1	D1 2	D2 3	D2 4	D2 5	DG 6
SiO_2	47.52	46.99	47.91	47.73	46.90	46.29
TiO_2	0.58	0.81	0.62	0.93	1.00	1.20
Al_2O_3	4.54	4.44	4.71	5.25	5.02	5.52
FeO_t	19.66	21.12	22.12	22.41	22.73	21.69
MnO	0.50	0.69	0.64	0.62	0.57	0.91
MgO	10.61	9.50	9.66	9.62	9.27	8.44
CaO	10.75	10.67	10.29	10.42	10.25	10.76
Na_2O	1.26	1.11	1.14	1.36	1.32	1.28
K_2O	0.46	0.50	0.49	0.55	0.54	0.62
P_2O_5	0.02	0.04	0	0	0.08	0
F	0.51	0.27	0.43	0.47	0.51	0.10
Cl	0.01	0.02	0.05	0.02	0.03	0.07
-F, Cl=0	0.22	0.12	0.19	0.20	0.22	0.06
TOTAL	96.20	96.04	97.87	99.18	98.00	96.82
Al-Factor	-0.325	-0.325	-0.298	-0.301	-0.297	-0.332
Fe-Factor	0.503	0.546	0.556	0.557	0.569	0.578

	AM	BIOTITE				
	DG	D1 2	D2 3	D2 4	D2 5	DG
SiO_2	46.63	31.89	36.55	35.63	35.92	35.83
TiO_2	1.32	3.59	3.79	4.38	3.85	4.30
Al_2O_3	5.64	12.83	12.77	12.68	12.51	12.58
FeO_t	21.47	24.02	23.67	24.09	28.85	23.39
MnO	0.83	0.31	0.27	0.24	0.47	0.45
MgO	8.35	9.10	8.95	8.47	8.47	7.97
CaO	10.88	0	0	0	0	0.02
Na_2O	1.35	0.08	0.07	0.10	0.12	0.08
K_2O	0.64	9.65	9.68	9.67	9.24	9.23
P_2O_5	0.02	0.02	0	0.01	0.01	0.03
F	0.07	0.73	0.83	0.70	0.15	0
Cl	0.07	0.07	0.10	0.06	0.07	0.07
-F, Cl=0	0.04	0.32	0.37	0.31	0.09	0.02
TOTAL	97.23	91.97	96.31	95.72	94.57	93.93
Al-Factor	-0.341	0.044	0.042	0.041	0.046	0.052
Fe-Factor	0.577	0.562	0.560	0.572	0.575	0.579

TABLE 2
(Continued)

INCLUSION (E)

	AMPHIBOLE										
	E2 1	E2 2	E3 3	E3 4	E4 5	E4 6	E5 7	E5 8	E5 8a	EG 9	EG
SiO_2	45.78	46.06	47.38	47.83	47.19	45.51	47.15	48.47	47.81	44.36	44.99
TiO_2	1.68	1.47	1.28	0.95	1.33	1.17	1.18	0.25	1.28	1.21	1.21
Al_2O_3	6.36	5.78	5.59	4.98	5.79	6.62	5.90	4.58	6.05	7.28	7.21
FeO_t	16.06	16.20	16.04	16.21	15.98	16.40	16.44	15.13	16.28	15.60	17.06
MnO	0.52	0.49	0.57	0.58	0.50	0.50	0.49	0.43	0.37	0.31	0.33
MgO	11.63	10.79	12.03	12.84	12.04	10.97	11.68	13.15	12.36	13.15	11.28
CaO	11.66	11.66	11.18	11.82	11.45	11.49	11.61	11.81	11.01	11.56	11.55
Na_2O	1.16	1.34	1.24	0.74	1.22	1.33	1.09	0.64	1.31	0.79	1.17
K_2O	0.54	0.69	0.48	0.42	0.49	0.65	0.63	0.24	0.54	0.41	0.65
P_2O_5	0.08	0.04	0.07	0.07	0.05	0.12	0.01	0.01	0.04	0.03	0.07
F	0.34	0.11	0.05	0.09	0.23	0.18	0.26	0.01	0.31	0.20	0.22
Cl	0.01	0.03	0.02	0.03	0	0.03	0.03	0.10	0.04	0.05	0.04
-F, Cl=0	0.14	0.05	0.03	0.04	0.10	0.08	0.12	0.03	0.14	0.10	0.10
TOTAL	95.68	94.61	95.90	96.52	96.17	94.89	96.35	94.79	97.26	94.85	95.68
Al-Factor	-0.342	-0.378	-0.332	-0.332	-0.339	-0.341	-0.344	-0.334	-0.315	-0.286	-0.317
Fe-Factor	0.412	0.436	0.410	0.402	0.408	0.440	0.425	0.389	0.407	0.382	0.443

	BIOTITE									
	E2 1	E2 2	E3 3	E3 4	E4 5	E4 6	E5 7	E5 8	EG 9	EG
SiO_2	35.82	35.79	35.60	35.90	35.48	35.58	35.20	36.08	35.72	35.01
TiO_2	3.28	4.37	4.54	3.98	4.46	4.51	4.12	3.51	4.47	4.28
Al_2O_3	13.52	12.88	13.08	12.97	13.19	12.91	13.10	13.45	13.48	12.99
FeO_t	20.39	20.25	20.55	20.81	20.44	20.00	20.63	20.46	20.31	19.79
MnO	0.33	0.26	0.28	0.30	0.18	0.29	0.27	0.29	0.22	0.30
MgO	10.40	10.39	10.68	10.81	10.42	10.80	10.66	10.58	10.94	10.49
CaO	0	0	0	0	0	0	0	0	0	0
Na_2O	0.06	0.09	0.06	0.11	0.07	0.12	0.08	0.10	0.09	0.14
K_2O	9.84	9.69	9.72	9.85	9.89	9.72	9.59	9.54	9.73	9.43
P_2O_5	0.06	0.14	0	0	0	0.06	0.03	0.03	0.02	0
F	0.21	0.23	0.28	0.29	0.19	0.29	0.22	0.22	0.25	0.37
Cl	0.17	0.12	0.16	0.17	0.12	0.18	0.06	0.21	0.04	0.16
-F, Cl=0	0.13	0.12	0.15	0.16	0.11	0.16	0.11	0.14	0.12	0.19
TOTAL	93.95	94.09	94.80	95.03	94.31	94.30	93.85	94.33	95.15	92.77
Al-Factor	0.054	0.045	0.049	0.041	0.048	0.044	0.051	0.058	0.055	0.052
Fe-Factor	0.485	0.468	0.464	0.472	0.469	0.453	0.471	0.479	0.455	0.460

TABLE 2
(Continued)

INCLUSION (F)

	AMPHIBOLE								
	F2 1	F2 2	F3 3	F3 4	F4 5	F4 6	F5 7	F5 8	FG
SiO_2	44.97	50.45	48.22	45.38	48.36	48.71	47.49	45.52	46.94
TiO_2	0.50	0.62	1.16	1.63	0.54	0.68	1.34	1.58	1.30
Al_2O_3	6.73	2.78	4.88	6.67	4.77	4.59	4.83	6.83	6.21
FeO_t	16.25	15.34	15.55	16.80	16.78	16.06	16.15	16.40	16.18
MnO	0.49	0.49	0.46	0.49	0.50	0.50	0.49	0.49	0.52
MgO	10.83	12.56	12.37	10.94	13.00	12.28	12.04	11.28	11.85
CaO	11.63	11.86	11.72	11.58	11.75	11.66	11.89	11.81	11.23
Na_2O	1.08	0.53	1.17	1.20	0.71	0.76	0.83	1.35	1.29
K_2O	0.69	0.30	0.56	0.67	0.31	0.47	0.46	0.65	0.44
P_2O_5	0.03	0.05	0.06	0	0.03	0.02	0.06	0.08	0.04
F	0.21	0.29	0.22	0.13	0.05	0.26	0.02	0.12	0.17
Cl	0	0.03	0.02	0.07	0	0.02	0.01	0	0.05
-F, Cl=0	0.09	0.13	0.10	0.07	0.02	0.12	0.01	0.05	0.07
TOTAL	93.32	95.17	96.29	95.56	96.78	95.89	95.60	96.06	96.15
Al-Factor	-0.339	-0.377	-0.363	-0.346	-0.322	-0.346	-0.358	-0.349	-0.326
Fe-Factor	0.450	0.398	0.397	0.440	0.413	0.414	0.411	0.427	0.415

	BIOTITE								
	F2 1	F2 2	F3 3	F3 4	F4 5	F4 6	F5 7	F5 8	FG
SiO_2	35.55	34.87	35.22	35.46	35.86	35.96	35.20	34.79	35.43
TiO_2	4.37	4.59	4.62	4.82	4.06	4.69	4.12	4.48	4.56
Al_2O_3	13.31	13.26	13.67	13.15	13.19	13.42	13.48	12.87	13.52
FeO_t	19.59	20.31	19.75	20.43	19.92	20.29	20.33	19.78	21.19
MnO	0.28	0.27	0.27	0.18	0.27	0.30	0.40	0.26	0.35
MgO	10.56	10.08	10.72	10.20	10.83	10.12	10.32	10.27	10.53
CaO	0	0	0.03	0	0.01	0	0	0	0
Na_2O	0.10	0.11	0.09	0.11	0.10	0.09	0.07	0.08	0.09
K_2O	9.65	9.74	9.79	9.79	9.94	9.65	9.68	9.37	9.36
P_2O_5	0	0.06	0.02	0.01	0.03	0	0.01	0.06	0.01
F	0.23	0.40	0.48	0.25	0.17	0.19	0.22	0.27	0.38
Cl	0.05	0.05	0.05	0.07	0.03	0.06	0.04	0.04	0.04
-F, Cl=0	0.11	0.18	0.21	0.12	0.08	0.09	0.10	0.12	0.17
TOTAL	93.58	93.56	94.50	94.35	94.33	94.68	93.77	92.15	95.29
Al-Factor	0.055	0.052	0.059	0.049	0.046	0.058	0.058	0.054	0.064
Fe-Factor	0.454	0.474	0.449	0.470	0.457	0.471	0.475	0.463	0.477

glasses. The basis for mathematical treatments of diffusion is Fick's first law, which applies to steady state diffusion:

$$J_i = D_i \frac{\delta \mu i}{\delta x} \quad (1)$$

where J_i is the flux, Di the diffusion coefficient, and $\delta\mu_i/\delta x$ the chemical potential gradient for component 1 over distance dx. For the major rock-forming cations the diffusion coeffient appears to decrease with increasing positive charge (for example, Borom and Pask, 1968). Thus with a constant potential gradient the flux for the more highly charged species will be lower compared to the species with lower charges. On the diagrams in figure 2 the change in composition for a reaction zone sample is directly related to the flux for each component with respect to either of the end compositions. It can be seen from the SiO_2–TiO_2–Al_2O_3 diagrams that for each enclave TiO_2 has the lowest flux. The same result is found for a similar plot of TiO_2, Zr, and V (table 1). Hence, TiO_2 is selected as the reference component. Also, TiO_2 is present in sufficient amounts in each inclusion-granite system to be determined accurately at wt percent levels. In addition, Ti_{4+} can be readily accommodated in the mafic silicates and opaques that form upon reaction between enclave and magma. The composition for the core of each enclave is considered to be closest to the initial composition for that enclave. Furthermore, in the diffusion process, the melt is probably the main medium for mass transfer, unless there was an aqueous fluid phase present, a situation more likely postdating crystallization. Changes in the concentration of elements across the reaction zone are therefore expressed relative to the core composition.

The molar proportions of the introduced and removed species in the reaction rim may be calculated if TiO_2 is assumed immobile. Reactions can be written to explain the change in mineralogy across the core-rim contact, knowing which components have been transferred with respect to TiO_2. If the additional assumption is made that TiO_2 on either side of the core-rim contact has been immobile (that is, flux = 0), then the molecular proportions of the mobile components can be determined. Calculated molecular proportions of the major elements (as the oxide component) are listed in table 3 for each of the inclusions. The reactions given in the next section have been written to correspond as closely as possible with both the data in table 3 and the modal data.

ENCLAVE DESCRIPTIONS

Enclave (A).—Whole rock and mineral compositions for enclave (A) are plotted in figure 3A. Of all the inclusions, this shows the largest difference in composition between core and host granite. Its core composition and mineralogy (table 1) and the layered texture (fig. 1A) indicate that this inclusion probably represents a xenolith of a carbonate-rich rock. On the diagram, core (A1) plots below the corresponding

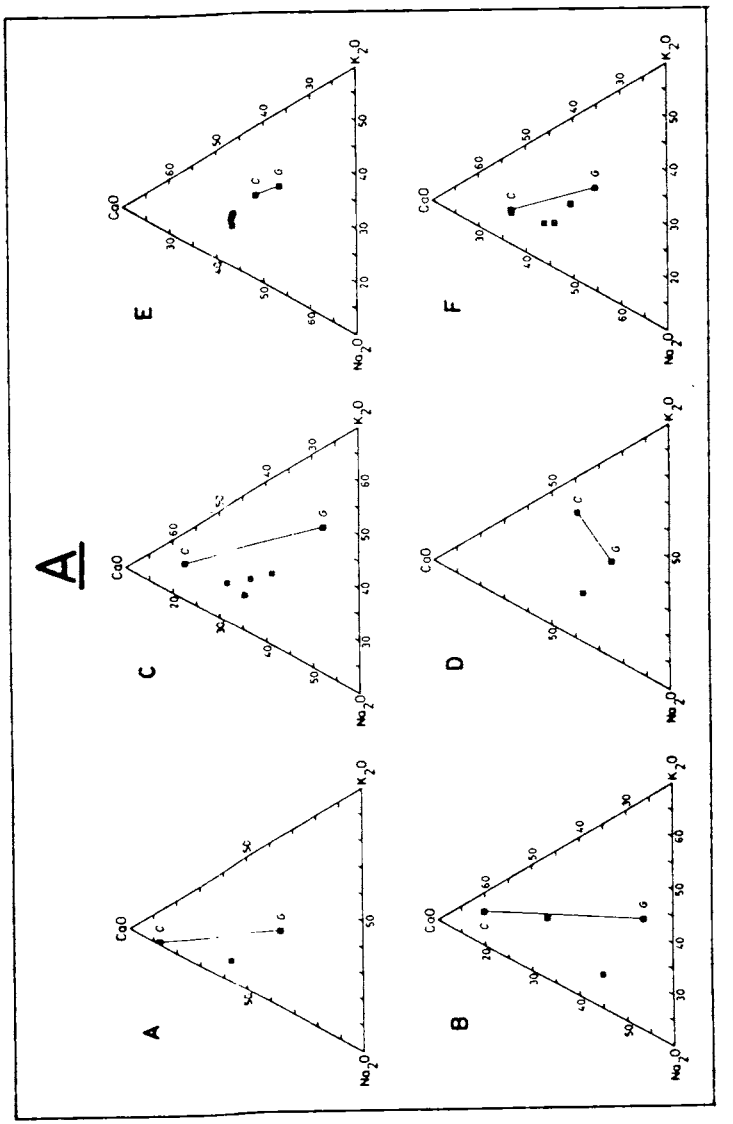
A
A
B
C
D
E
F
CaO
K_2O
Na_2O
C
G

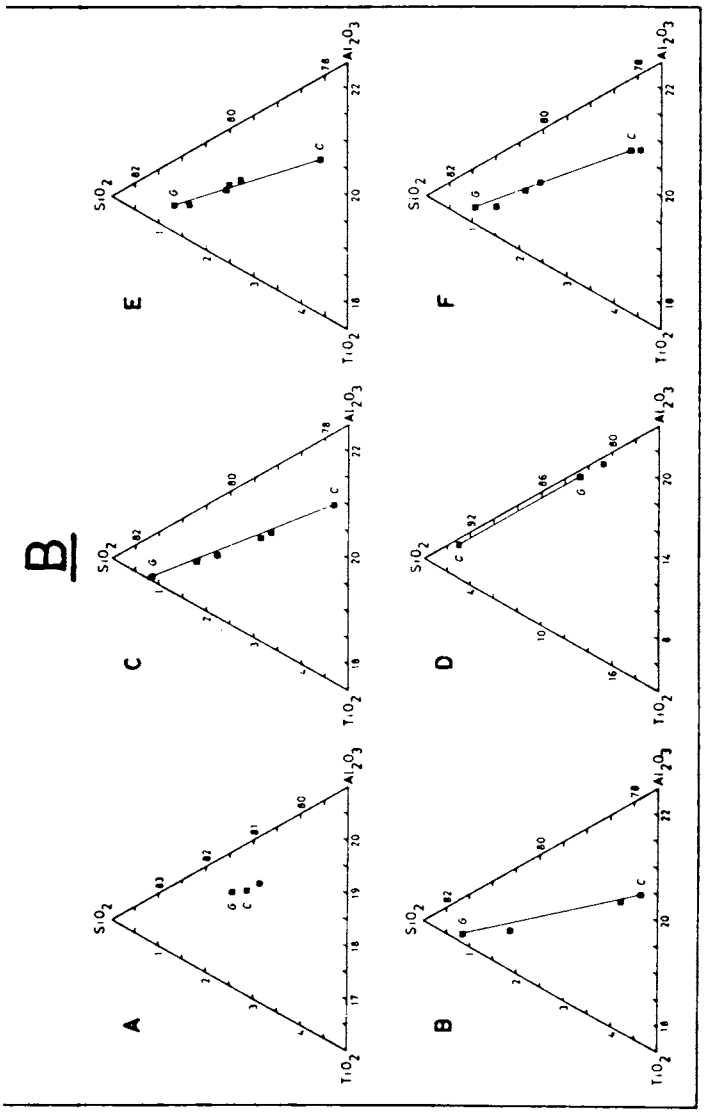

Fig. 2(A) CaO–Na_2O–K_2O (wt percent) diagrams. (B) SiO_2–TiO_2–Al_2O_3 (wt percent) diagrams for bulk rock samples from enclaves (A) to (F). Plots for the reaction rim samples show a distinct deviation from the straight lines (mixing lines) between the cores (C) and the granites (G). Compositions for the low charged species 7(A) compared with those for the high charged species (7B).

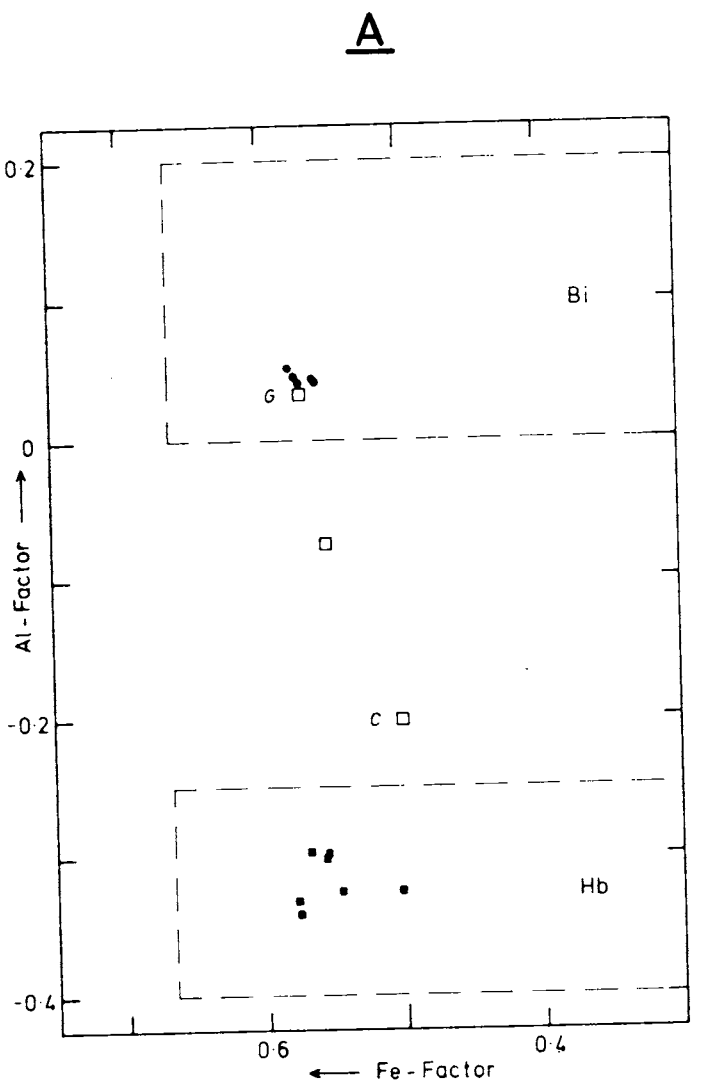

Fig. 3(A) Modified AFM diagram after Thompson, 1957 for enclave (A) showing bulk rock compositions (open squares; C = core and G = granite) and mineral compositions (solid symbols: circles = biotite (Bi), squares = hornblende (Hb), and diamonds = diopside (Di)). For dashed lines see figure 1(B).

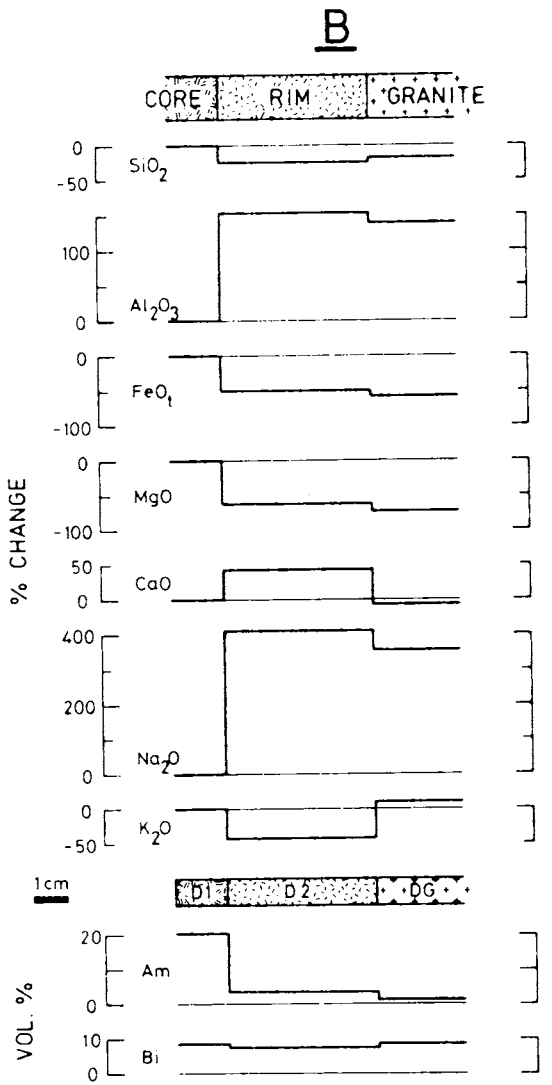

Fig. 3 (continued)
(B) Bulk rock chemical variations of major elements, and modes for diopside, amphibole, and biotite, across the sample profile of enclave (A). The variation of a component is given as the percent change relative to the core composition, with respect to a TiO_2-reference frame. Average values for sample sections are plotted without smoothing.

A

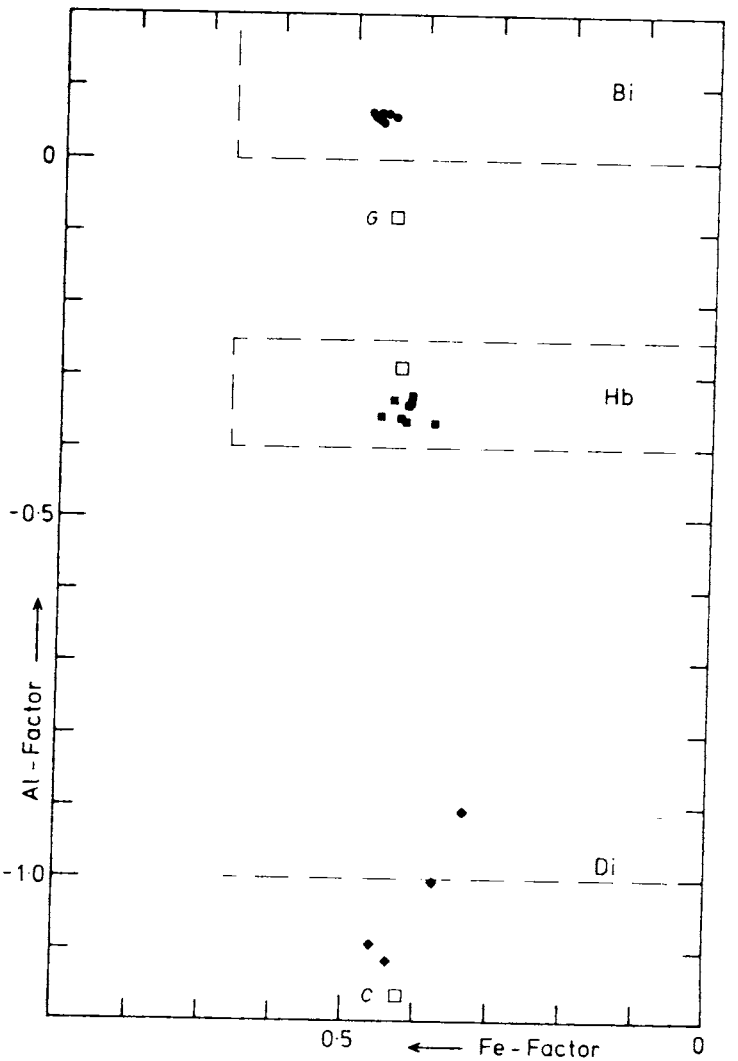

Al-Factor = $(Al_2O_3 - CaO - Na_2O - K_2O)/(FeO_t + MgO)$

Fe-Factor = $FeO_t/(FeO_t + MgO)$

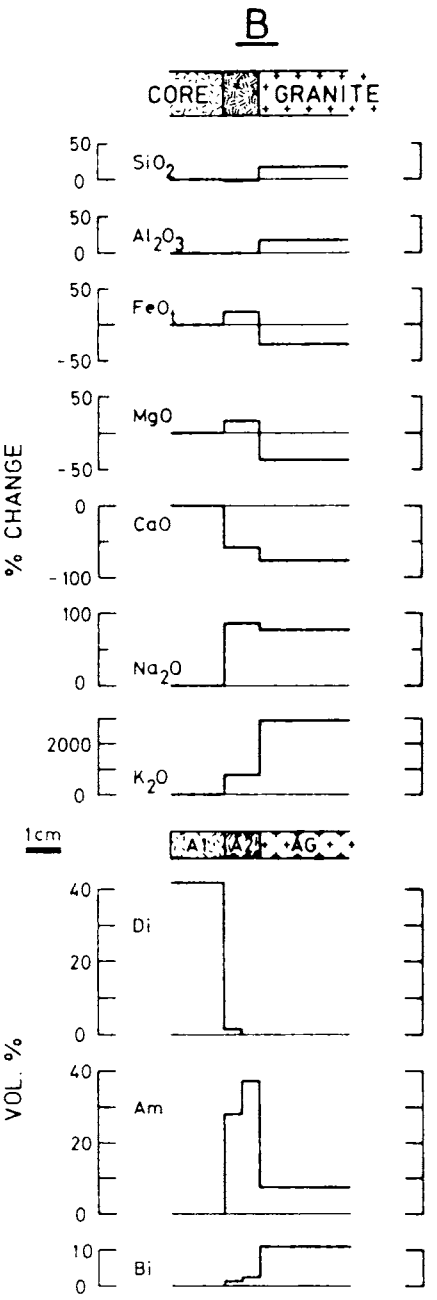

Fig. 4(A) Modified AFM diagram showing bulk rock and mineral compositions for enclave (B). Symbols: large open squares = bulk rock compositions, inverted triangles = cordierite (Co), triangles = garnet (Gt) circles = biotite, and small open squares = anthophyllite (see also fig. 1D); for further explanation see figure 3A. (B) Bulk rock chemical variations of major elements and modes for amphibole, biotite, garnet, and cordierite. For further explanation see figure 3B.

A

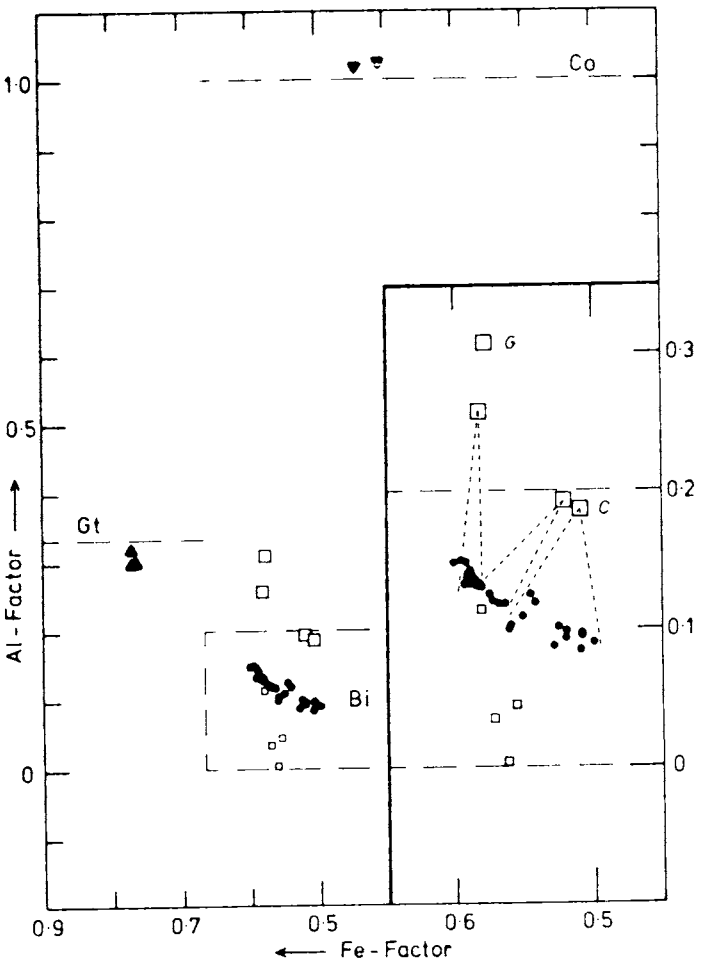

Fig. 5(A) Modified AFM diagram showing bulk rock and mineral compositions for enclave (C). Symbols: open squares = bulk rock compositions, circles = biotite, and solid squares = amphibole. For further explanation see fig. 3A.

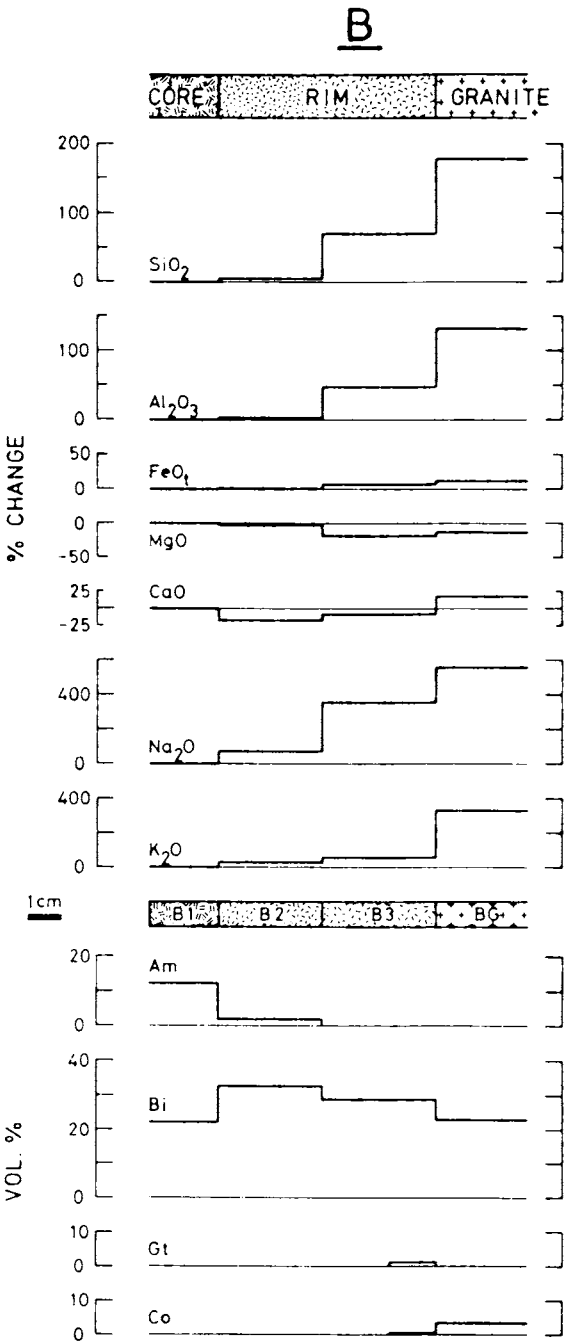

Fig. 5 (continued)
(B) Bulk rock chemical variations of major elements and modes for amphibole and biotite. For further explanation see figure 3B.

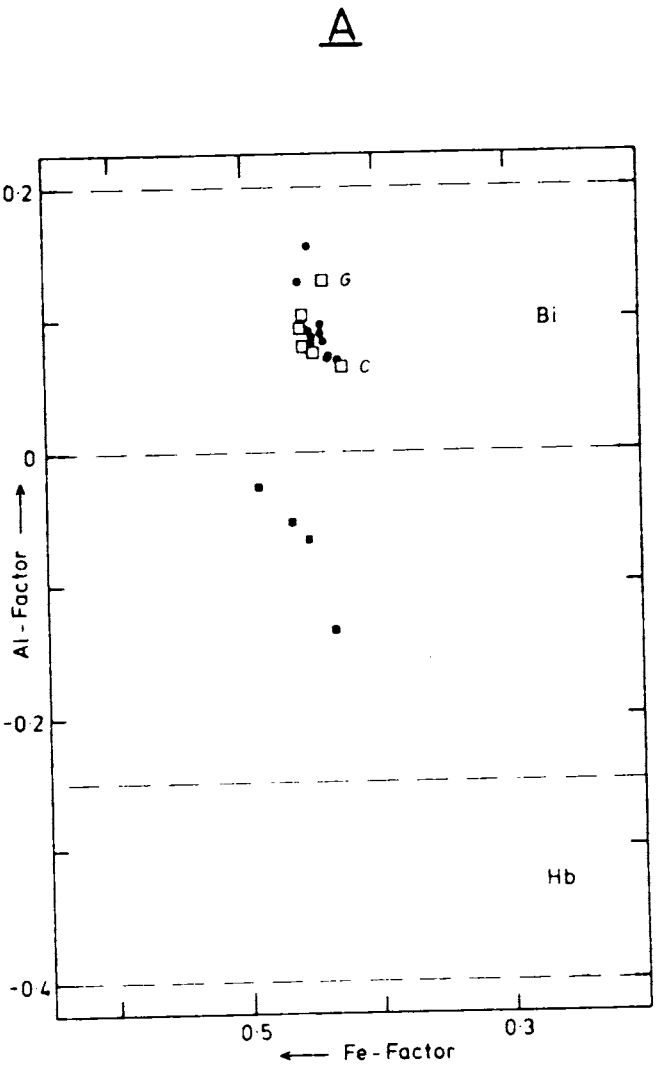

Fig. 6(A) Modified AFM diagram showing bulk rock and mineral compositions for enclave (D). Symbols: open squares = bulk rock compositions, circles = biotite, and solid squares = amphibole. For further explanation see figure 3A.

diopside analyses because the Al-factor is not corrected for CO_2 (that is, for calcium in carbonate minerals). The amphibole (hornblende)-rich reaction zone (A2) plots close to the mixing line between granite and core, and the corresponding amphibole compositions do not appear to be related to the changing bulk composition across the sample profile.

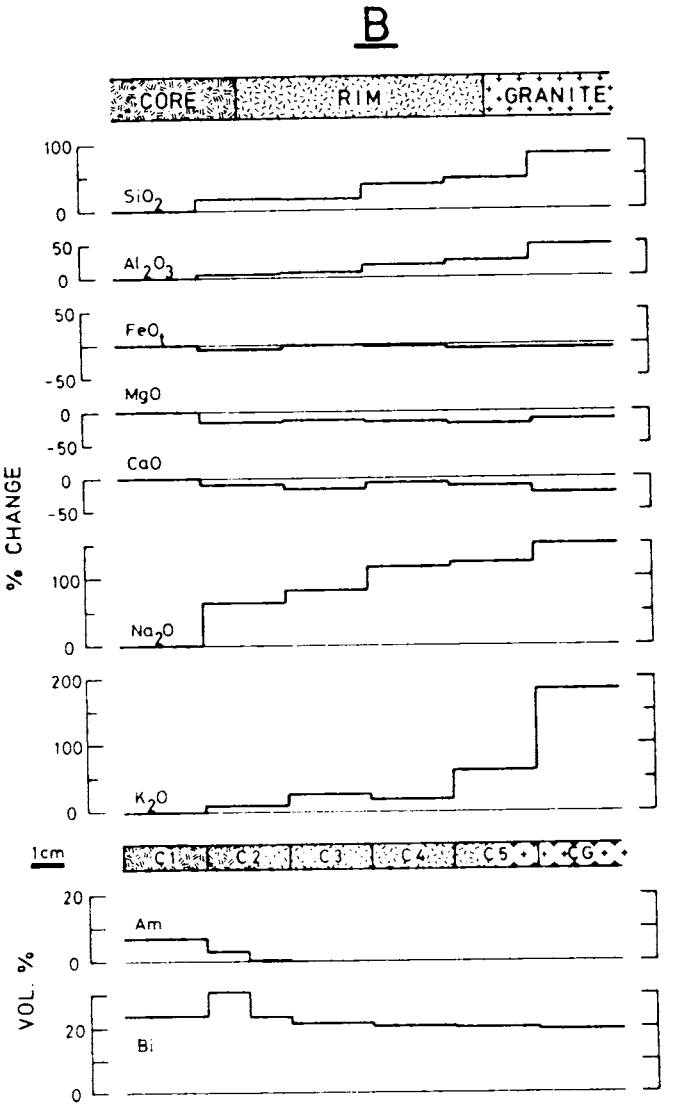

Fig. 6 (continued)
(B) Bulk rock chemical variations of major elements and modes for amphibole and biotite. For further explanation see figure 3B.

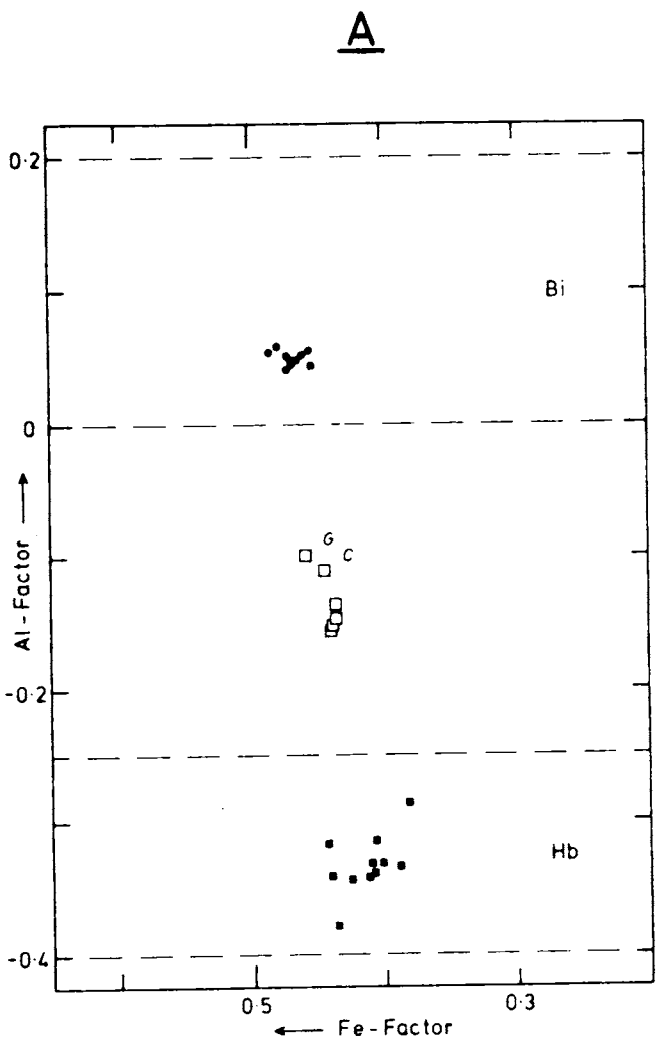

Fig. 7(A) Modified AFM diagram showing bulk rock and mineral compositions for enclave (E). Symbols are: open squares = bulk rock compositions, circles = biotite, and solid squares = amphibole. For further explanation see figure 3A.

However, this *apparent* mixing relationship is contradicted by the plots in figure 2. The linear bulk rock trend in figure 3A is probably the result of both core (A1) and the granite having almost identical Fe-factors. Fe and Mg appear to have the same flux during diffusion (see fig. 3B). Thus the Fe-factor for the reaction rim (A2) is not much different from the values for the core and the granite. Additional evidence for diffusion is shown by the change in diopside composition between points 1 and 4

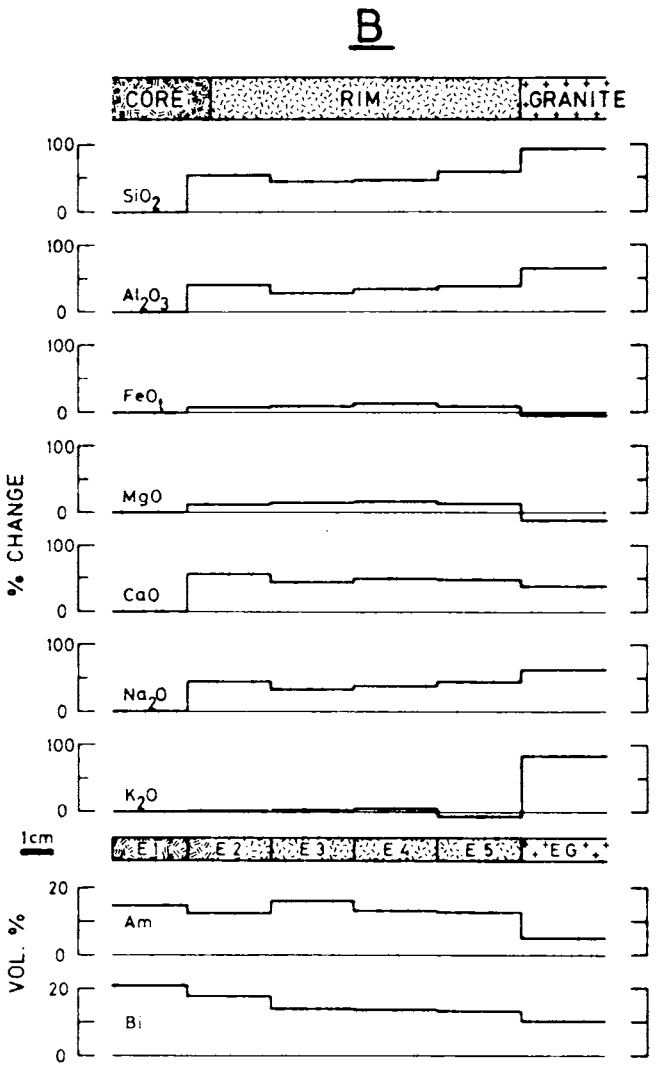

Fig. 7 (continued)
(B) Bulk rock chemical variations of major elements, and modes for amphibole and biotite. For further explanation see figure 3B.

(see fig. 1). This change corresponds to a decrease in CaO and an increase in Na_2O contents (table 2) without a significant increase in the Al_2O_3 content as the reaction rim is approached. These data are supported by the trends in figure 3B.

The chemical variation across the reaction zone is shown schematically in figure 3B. In the lower part of the diagram, the modal

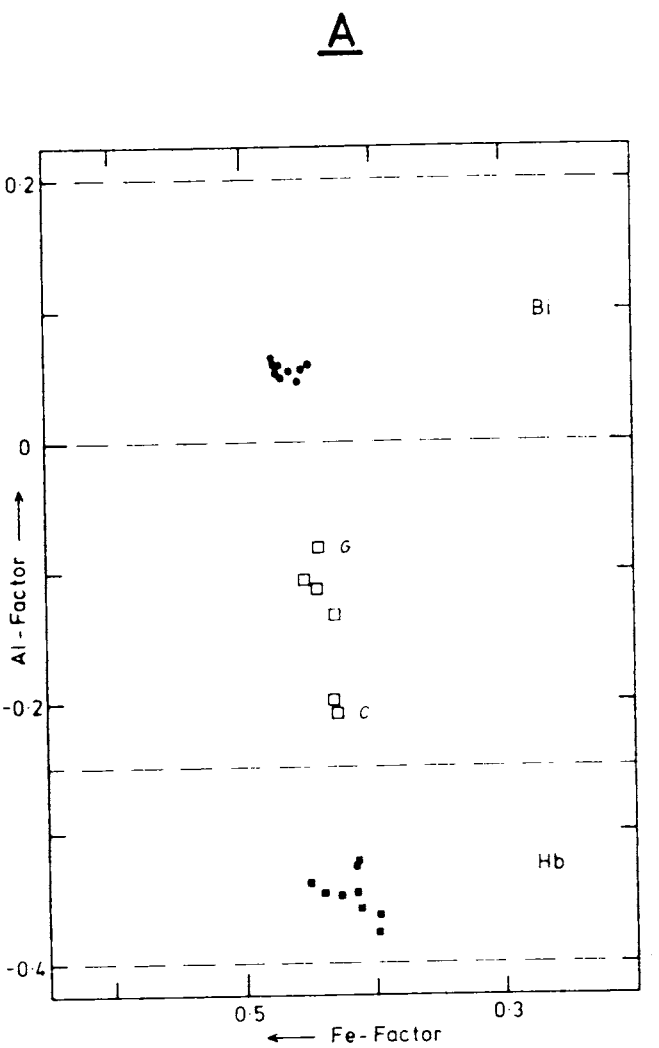

Fig. 8 (A) Modified AFM diagram showing bulk rock and mineral compositions for enclave (F). Symbols: open squares = bulk rock compositions, circles = biotite, and solid squares = amphibole. For further explanation see figure 3A.

abundances for the major ferromagnesian silcates are plotted. Relative to the core, SiO_2 and Al_2O_3 remain constant, whereas FeO_t and MgO are both enriched to approximately the same extent in the reaction rim. CaO has been removed, and Na_2O and K_2O have been introduced into the rim. Using the compositions of the analyzed diopside and

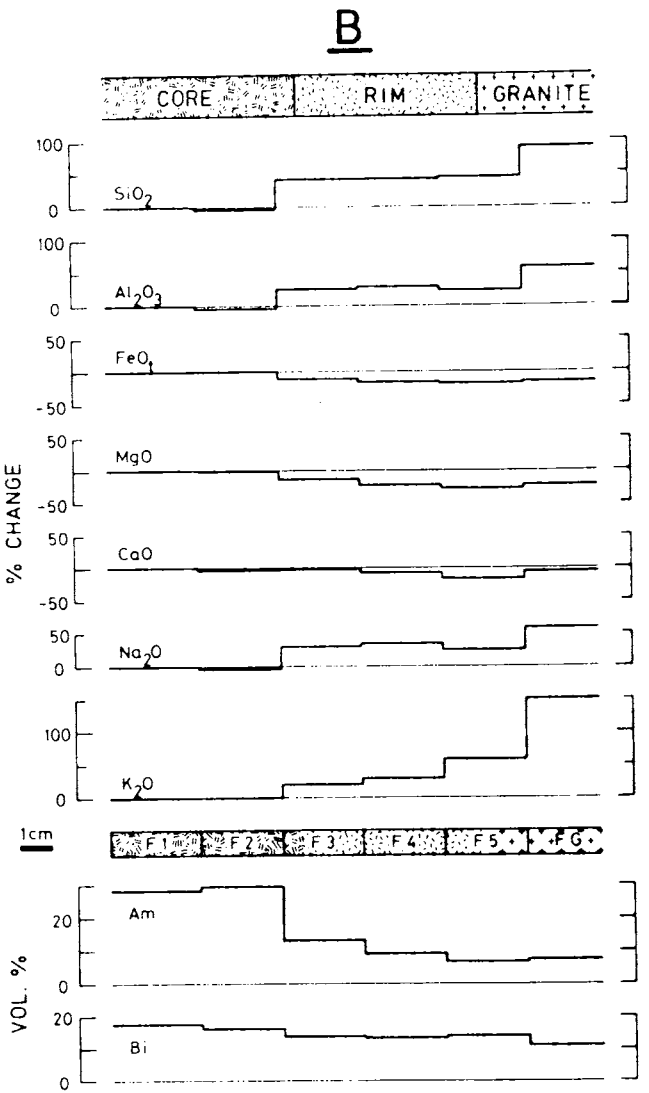

Fig. 8 (continued)
(B) Bulk rock chemical variations of major elements and modes for amphibole and biotite. For further explanation see figure 3B.

amphibole, the following reaction may be written to explain the observed mineralogical changes for the reaction rim:

Reaction 1

$$\underset{\text{diopside}}{12Ca(Fe, Mg)Si_2O_6} + \underset{\text{anorthite}}{4CaAl_2O_8} + \underset{\text{carbonate}}{5CaCO_3} + \underset{\text{quartz}}{6SiO_2} + \left\{\begin{matrix} 3(FeO, MgO) \\ 3Na_2O \\ K_2O \\ 3H_2O \\ O_2 \end{matrix}\right.$$

introduced

$$\rightleftharpoons$$

$$\underset{\text{hornblende}}{3(Na, K)Ca_2(Fe, Mg)_5Si_7A1_{22}(CH)_2} + \underset{\text{alkali-feldspar}}{5(Na, K)AlSi_3O_8} + \left\{\begin{matrix} 2SiO_2 \\ 17CaO \\ 5CO_2 \end{matrix}\right.$$

removed

Biotite in the rim is mainly seen to have nucleated on amphibole, so that biotite is not included in reaction 1. With diffusion, both the composition of the inclusion and of the immediate granite contact are affected, so that the initial boundary probably lies somewhere within the present rim A2. This is supported by the separate modal data for the inner and outer half of (A2). Diopside occurs only in the inner half of the rim along the contact with the core. The higher amphibole abundance in the outer part of (A2) could thus also be the result of CaO (see eq 1) being introduced. Furthermore, biotite in the rim near the contact with

TABLE 3

Stoichiometry (in molecular proportions) of major element components that have been introduced (+) / or removed (−) from the reaction rim adjacent to the core-rim contact calculated on the basis of TiO_2 remaining constant relative to the core

	A2	B2	B3	C2	C3
SiO_2	−1.8	+7.5	+53.1	+32.8	+23.5
Al_2O_3	+0.02	+0.06	+5.5	+2.0	+1.8
FeO_t	+1.4	+0.1	+0.6	−1.0	−0.1
MgO	+1.4	−0.4	−1.2	−3.0	−1.8
CaO	−17.0	−2.4	−0.6	−1.8	−2.4
Na_2O	+3.1	+1.9	+4.6	+3.2	+2.9
K_2O	+1.0	+1.0	+1.0	+0.5	+1.0
	D2	E2	E3	F3	F4
SiO_2	−26.1	+20.4	+22.6	+98.2	+67.4
Al_2O_3	+6.3	+2.3	+2.3	+9.1	+6.9
FeO_t	−3.0	+0.3	+0.5	−2.9	−2.7
MgO	−3.5	+0.5	+0.8	−4.1	−4.6
CaO	+1.3	+1.8	+1.9	−1.1	−1.6
Na_2O	+4.1	+1.0	+1.0	+4.5	+3.4
K_2O	−1.0	0	0	+1.0	+1.0

the granite also occurs as larger, separate crystals. Hence, the fact that the amphibole compositions on figure 3A show no clear relationship with the bulk compositional trend may be the result of the initial granite-inclusion boundary lying within the reaction zone.

Enclave (B).—Whole-rock and mineral compositions for enclave (B) which may well be a xenolithic enclave are plotted on diagram A in figure 4. In this inclusion, the mineral assemblage changes from anthophyllite + biotite to garnet + cordierite + biotite. The open symbols for anthophyllite in figure 4A indicate that the compositions for this mineral actually plot below the projection surface of the diagram (see fig. 1D). The core (B1) and the granite (BG) both have different Fe-factors as well as Al-factors. Across the reaction zone changes in bulk rock composition are closely related to changes in the composition of biotite as illustrated in the enlarged section of the diagram (inset fig. 4A). Within the core (B1), chemical variations are also shown by the changing anthophyllite composition. For this mineral, the change corresponds (table 2) to an increase in Al_2O_3 and a decrease in both FeO_t and MgO. A similar trend for Al_2O_3 and MgO is shown by the 27 biotite analyses across the zoned inclusion, but the FeO_t content shows a slight overall increase toward the outer contact. As a result of these opposite trends for FeO_t and MgO, the bulk core Fe-factor increases in the outer zone (B3) to a value such that garnet becomes a stable phase in addition to cordierite. The host granite, with a Fe-factor slightly lower than B3, contains only cordierite. The correlations between compositional trends for bulk rock and minerals, as well as the bulk rock trends in figure 2, imply that mass transfer has been controlled largely by diffusion.

Variations in major element concentrations and the modal abundances of the characteristic minerals for inclusion (B) are illustrated in figure 4B. Appreciable Na_2O, K_2O, SiO_2, and Al_2O_3, and some FeO, have been introduced in the rim. CaO has been depleted, and MgO has been removed from the rim, relative to the core composition. Calcic plagioclase is the dominant feldspare in the core (see fig. 1B), whereas, in the rim, K-feldspar is common. Thus, the following reaction is written to explain the disappearance of anthophyllite in the reaction zone:

Reaction 2

$$\underset{\text{anthophyllite}}{(Fe, Mg)_7Si_8O_{22}(OH)_2} + \underset{\text{anorthite}}{5CaAl_2Si_2O_8} + \underset{\text{introduced}}{\begin{cases} 18SiO_2 \\ Al_2O_3 \\ 4Na_2O \\ 2K_2O \\ H_2O \end{cases}} =$$

$$\underset{\text{biotite}}{K_2(Fe, Mg)_6Al_2Si_6O_{20}(OH)_4} + \underset{\text{orthoclase}}{2KAlSi_3O_8} + \underset{\text{albite}}{8NaAlSi_3O_8} + \underset{\text{removed}}{\begin{cases} MgO \\ 5CaO \end{cases}}$$

However, the present core composition may not represent the composition of the original inclusion but may be a reaction product similar to the present rim of the inclusion. A reaction can be written assuming diffusion of the same components as in reaction (2) to derive orthoamphibole (anthophyllite) from an orthopyroxene + Ca-plagioclase assemblage.

Reaction 3

$$\underset{\text{orthopyroxene}}{10(Fe, Mg)_2Si_2O_6} + \underset{\text{anorthite}}{5CaAl_2Si_2O_8} + \left\{\begin{matrix}18SiO_2\\Al_2O_3\\4Na_2O\\2K_2O\\5H_2O\end{matrix}\right.\ \text{introduced}$$

$$=$$

$$\underset{\text{anthophyllite}}{(Fe, Mg)_7Si_8O_{22}(OH)_2} + \underset{\text{biotite}}{2K_2(Fe, Mg)_6Al_2Si_6O_{20}(OH)_4}$$

$$+ \underset{\text{albite}}{8NaAlSi_3O_8} + \underset{\text{quartz}}{4SiO_2} + \left\{\begin{matrix}MgO\\5CaO\end{matrix}\right.\ \text{removed}$$

Compared with reaction 2 this reaction only requires a higher flux for H_2O. The importance of reaction 3 with respect to mass balance reactions lies in the removal of CaO from the inclusion. The removal of a component, relative to the initial composition, can occur only if it has a negative chemical potential gradient from the inclusion toward the granite. Evidence for the existence of such an initial CaO chemical potential gradient is given by the plagioclase compositions and textures across the core-rim section (see fig. 1B).

Enclave (C).—The bulk rock compositions for enclave (C) and its host granite plot wholly within the biotite stability field (fig. 5A). However, the core of this inclusion contains a Ca-poor clinoamphibole which, on the basis of its texture and intergrowth with Ca-plagioclase (see fig. 1C), probably represents a metastable phase. Across the reaction zone the bulk rock composition changes systematically resulting in a distinctly curved trend. On the diagram this trend is related to the changing biotite and amphibole compositions. The variation in amphibole composition (table 2) corresponds to a decrease in MgO and CaO contents and an increase in FeO_t content, whereas Al_2O_3 shows no systematic change upon approaching the reaction rim. The biotite trend results from an increase in AL_2O_3 and a decrease in MgO contents, whereas FeO_t remains virtually unchanged. As a result, the whole-rock Fe-factors for the rim are higher than for both the core (C1) and the granite (CG). Furthermore, with respect to the other major elements the

bulk rock trends for inclusion C (fig. 2) show similar non-linear variations. This indicates that diffusion was involved in the mass transfer between granite and enclave.

Figure 5B illustrates the chemical variation across the reaction zone of enclave (C). With respect to the core, appreciable Na_2O has been introduced in addition to SiO_2, Al_2O_3, and K_2O, whereas MgO and CaO have been removed. FeO_t is virtually unchanged relative to the core. Using these data and the observed mineral textures (see fig. 1C), the following reaction may be written for the disappearance of amphibole in the reaction rim:

Reaction 4

$$\underset{\text{Ca-poor clinoamphibole}}{(Fe, Mg)_7Si_8O_{22}(OH)_2} + \underset{\text{anorthite}}{2CaAl_2Si_2O_8} + \left\{\begin{matrix} 28SiO_2 \\ Al_2O_3 \\ 3Na_2O \\ K_2O \end{matrix}\right. \text{introduced}$$

$$\rightleftharpoons$$

$$0.5K_2(Fe, Mg)_6Al_2Si_6O_{20}(OH)_4 + 6NaAlSi_3O_8 + KAlSi_3O_8 + 16SiO_2 + \left\{\begin{matrix} FeO \\ 3MgO \\ 2CaO \end{matrix}\right. \text{removed}$$

This reaction is similar to reaction 2 with the exception that some FeO is introduced and more MgO is removed from enclave B. This is probably a result of the greater difference in Fe and Mg contents for the core of inclusion B and its host granite. By analogy with the previous enclave, the Ca-poor clinoamphibole in the core (C1) may have formed from an initial orthopyroxene + Ca-plagioclase assemblage/via a reaction similar to reaction 3. The poikilitic fabric of the core, with euhedral laths of labradorite, suggests the possibility of a volcanic origin for inclusion (C), in which case the clinoamphibole could be primary (Deer, Howie, and Zussman 1974).

Enclave (D).—Whole-rock and mineral compositions for enclave D are plotted on diagram A in figure 6. Compared with the other inclusions, this enclave has a different core composition, with high SiO_2 and low Al_2O_3. All Ca in the core is in the amphibole (hornblende) which, together with the low Na_2O, accounts for the scarcity of plagioclase (see fig. 1D). The amphibole-rich core and the reaction rim have a weak but distinct foliation (fig. 1D). This foliation and the anamalous core composition (compared to the granite) suggest this inclusion is probably a xenolith. It may still be a restite enclave and have an unusual bulk composition. The change in composition of amphibole and biotite

from the core (D1) to the granite (DG) is related to the variation in bulk rock composition. For amphibole, this change corresponds (table 2) to an increase in Al_2O_3 and FeO_t contents and a decrease in the MgO content, whereas CaO is lower for amphiboles in the rim relative to the amphiboles in both core and granite. The change in biotite composition is limited to MgO, which decreases in biotites as the granite is approached. Despite the limited number of samples for this inclusion, the bulk rock compositions (figs. 2 and 6A) show distinctly curved trends, indicating the importance of diffusion in the mass transfer.

For the reaction rim of enclave (D), the chemical variations and the modal data for amphibole and biotite are given in figure 6B. Relative to the cores, appreciable Na_2O and Al_2O_3 and some CaO have been introduced in the rim, whereas MgO, FeO_t, K_2O, and SiO_2 have been removed. The modal abundance of biotite in the rim is essentially the same as for the core and the granite. However, with respect to the core, the reaction rim contains less quartz, and it is considerably richer in plagioclase, particularly in the albite component (see fig. 1D). Using the above data plus the composition of the amphibole from the core, the following reaction is written to explain the observed change in mineralogy across the core-rim contact:

Reaction 5

$$\underset{\text{hornblende}}{NaCa_2(Fe, Mg)_5Si_7AlO_{22}(OH)_2} + 0.25\underset{\text{biotite}}{K_2(Fe, Mg)_6Al_2Si_6O_{20}(OH)_4}$$

$$+ \underset{\text{orthoclase}}{1.5KAlSi_3O_8} + \underset{\text{quartz}}{46SiO_2} + \underset{\text{introduced}}{\begin{cases} 6Al_2O_3 \\ CaO \\ 4Na_2O \end{cases}}$$

$$\rightleftharpoons$$

$$\underset{\text{albite}}{9NaAlSi_3O_8} + \underset{\text{anorthite}}{3CaAl_2Si_2O_8} + \underset{\text{removed}}{\begin{cases} 26SiO_2 \\ 3FeO \\ 3.5MgO \\ K_2O \\ 1.5H_2O \end{cases}}$$

This reaction implies a dehydration of the original enclave which, in this case, supports the classification of this enclave as a xenolith, rather than a restite or autolith enclave. Furthermore, the difference in structure of the plagioclase phenocrysts from the rim (normally zoned) and from the granite (complexly zoned with distinct cores) can be explained by reaction 5.

Enclaves (E) and (F)—Enclaves (E) and (F) are significantly different. Both are probably restite but may be autolithic or even xenolithic enclaves. Both are from different localities, and both contain the same mineral assemblage as the granite, namely biotite + amphibole (hornblende) with accessory primary sphene and ilmenite. In addition, both contain large plagioclase grains with similar structures and compositions, resembling those within the granite. The granites from both localities are very similar in composition (table 1). However, the amphibole/biotite ratio for enclave (E) increases from core to rim, whereas for enclave (F) this ratio decreases in the same direction. This is illustrated in figures 7A and 8A respectively. It is apparent from these diagrams and from the data in table 2 that the changes in amphibole and biotite compositions for these inclusions are not related to the bulk rock trend for that inclusion. Nevertheless, the curvature of the bulk rock trends in figures 2, 7A, and 8A indicate that diffusion has been the important mechanism of mass transfer for the formation of these reaction rims. These enclaves may also be autoliths (the cores).

Figures 7B and 8B illustrate the different chemical variations across the reaction zones of inclusions E and F. Relative to core (E1), all major elements, except K, have been introduced in the rim: K_2O has remained virtually unchanged with respect to TiO_2. For the rim of inclusion F, SiO_2, Al_2O_3, Na_2O, and K_2O have been introduced, and FeO_t, MgO, and some CaO have been removed. On the same diagrams the modal data for biotite show a similar trend for both inclusions, whereas the amphibole trends are distinctly different. Using the above data for inclusion (E), the following reaction is written to explain the different textures and mineral proportions across the core-rim contact (see fig. 1D):

Reaction 6

$$\underset{\text{biotite}}{0.5K_2(Fe, Mg)_6Al_2Si_6O_{20}(OH)_4} + \underset{\text{introduced}}{\begin{cases} 43SiO_2 \\ 4Al_2O_3 \\ 2(FeO, MgO) \\ 4CaO \\ 2Na_2O \end{cases}}$$

$$\rightleftharpoons$$

$$\underset{\text{hornblende}}{NaCa_2(Fe, Mg)_5AlSi_7O_{22}(OH)_2} + \underset{\text{anorthite}}{2CaAl_2Si_2O_8}$$

$$+ \underset{\text{albite}}{3NaAlSi_3O_8} + \underset{\text{orthoclase}}{KAlSi_3O_8} + \underset{\text{quartz}}{23SiO_2}$$

Similarly for inclusion (F) the lower emphibole content of the rim can be explained by reaction 7:

Reaction 7

$$\underset{\text{hornblende}}{2NaCa_2(Fe, Mg)_5AlSi_7O_{22}(OH)_2} + \underset{\text{introduced}}{\begin{cases}82SiO_2\\8Al_2O_3\\4Na_2O\\K_2O\end{cases}} \rightleftharpoons$$

$$\underset{\text{biotite}}{0.5K_2(Fe, Mg)_6Al_2Si_6O_{20}(OH)_4} + \underset{\text{anorthite}}{3CaAl_2Si_2O_8} + \underset{\text{albite}}{10NaAlSi_3O_8}$$

$$+ \underset{\text{orthoclase}}{KAlSi_3O_8} + \underset{\text{quartz}}{54SiO_2} + \underset{\text{removed}}{\begin{cases}3FeO\\4MgO\\CaO\\H_2O\end{cases}}$$

A comparison of these last two reactions with figures 7B and 8B illustrates the essential difference between the two inclusions with respect to CaO. In both inclusions the reaction rim contains more plagioclase than the core. However, plagioclase is more abundant in the core of enclave F compared with the core of enclave E (compare fig. 1D and E). This has an important implication with respect to the initial, high temperature, mineral assemblages of the original enclaves. As in the case for inclusion (B), reaction can be written using the same proportions of components as for reactions 6 and 7 to generate the hornblende assemblage of the present cores (E1) and (F1). However, as a result of the proportions for CaO and Al_2O_3 in reactions 6 and 7, such a reaction for the core of E (E1) can only be written with orthopyroxene and, for the core of F (F1), only with clinopyroxene. For inclusion (E) this is shown by reaction 8:

Reaction 8

$$1.5(Fe, Mg)_2Si_2O_6 + \underset{\text{introduced}}{\begin{cases}43SiO_2\\4Al_2O_3\\2(FeO, MgO)\\4CaO\\2Na_2O\\H_2O\end{cases}} \rightleftharpoons$$

$$\underset{\text{hornblende}}{NaCa_2(Fe, Mg)_5AlSi_7O_{22}(OH)_2} + \underset{\text{anorthite}}{2CaAl_2Si_2O_8}$$

$$+ \underset{\text{albite}}{3NaAlSi_3O_8} + \underset{\text{quartz}}{26SiO_2}$$

and for inclusion (F) by reaction 9.

Reaction 9

$$\underset{\text{clinopyroxene}}{6Ca(Fe, Mg)Si_2O_6} + \underset{\text{biotite}}{K_2(Fe, Mg)_6Al_2Si_6O_{20}(OH)_4} + \underset{\text{introduced}}{\begin{cases}82SiO_2\\8Al_2O_3\\4Na_2O\\K_2O\end{cases}}$$

$$=$$

$$\underset{\text{hornblende}}{NaCa_2(Fe, Mg)_5AlSi_7O_{22}(OH)_2} + \underset{\text{anorthite}}{3CaAl_2Si_2O_8} + \underset{\text{albite}}{7NaAlSi_3O_8}$$

$$+ 4KAlSi_3O_8 + 54SiO_2 + \underset{\text{removed}}{\begin{cases}3FeO\\4MgO\\CaO\\H_2O\end{cases}}$$

DISCUSSION OF RESULTS

Mineralogical and chemical data presented for the zoned enclaves suggest that the formation and composition of a reaction rim result from diffusion controlled mass transfer across the inclusion-magma interface. Although both mixing and diffusion can result in rim compositions intermediate between that of the granite and the cores of the enclave, the non-linear bulk rock trends (figs. 3-8) rule out mixing as the dominant mechanism. The correlation between mineral compositions (for biotite, amphibole, and pyroxene) and the change in bulk rock composition are indications of crystal growth in a system where concentration gradients are controlled by steady state-like diffusive process. Additional evidence for diffusion is illustrated by the applicability of the reactions (1–7) in interpreting the mineralogical observations. These reactions are based on the data from table 3.

Since the alteration recorded within an enclave represents a retrograde reaction, some insight may be gained as to the composition of the original, high-grade enclave when first included in the magma. Irrespective of the possible difference in source composition of a xenolith, autolith, or a restite enclave, both incorporated materials will initially have undergone retrograde alteration. Xenolithic materials will usually but not always reach their maximum temperature during incorporation by the magma, in which case temperatures may reach 800 °C or above. Restite inclusions will initially have high-grade assemblages compatible with that of the melting event. However, upon ascent and emplacement of the magma, reactions take place in which the mineral phases of the inclusion equilibrate or re-equilibrate under lower T P, or changing fo_2, et cetera conditions.

It is considered that these reactions are determined by diffusion controlled mass transfer where there was an appreciable bulk composition difference, otherwise the change will be due to differences of intensive parameter (P, T, fo_2, F_{H_2O}, et cetera). As an approximation of these initial gradients, the same stoichiometry of components for the present core-rim reaction (table 3) may be used to probe the possible assemblage of the original enclave. This is illustrated for enclave (B), (C), (E), and (F) by reactions (3, 4, 8, and 9) respectively.

In these reactions, given the particular stoichiometry, the possible high-grade assemblage appears to be determined by the molecular proportions CaO and Al_2O_3. For instance, in reaction 4, clinopyroxene instead of orthopyroxene would require either a larger amount of CaO to be removed or a higher proportion of Al_2O_3 to be introduced. Similarly, if hornblende were derived from orthopyroxene instead of clinopyroxene as in reaction 10, this would require introduction of either a smaller amount of Al_2O_3 or CaO as well as Al_2O_3.

However, using this approach, only a general indication of the original composition of the inclusion can be gained. Little may be said about its origin, since a mineral assemblage alone is an insufficient criterion for determination of origin. In some cases textural evidence is vital. This is particularly true for inclusion B. For instance, if inclusions (E) and (F) are restite enclaves, then reactions 9 and 10 could indicate that both an orthopyroxene- and a clinopyroxene-bearing assemblage were at some stage in equilibrium with the same magma (the Lysterfield Granodiorite). In this case, supporting evidence is found where orthopyroxene and rare clinopyroxene occur as phenocrysts and in mineral "clots" in the upper rhyodacite from the associated Mt. Dandenong volcanic sequence. Here clinopyroxene is also present as a relict phase in some of the associated porphyritic dikes within the granodiorite pluton (see Cramer, ms, chap. 5). On the other hand, enclave (E) was collected from the intrusive contact of the granodiorite with the orthopyroxene-bearing rhyodacite (see Cramer, ms, fig. 5.1, loc. 43). Hence, a possibility exists that enclave (E) is a xenolith enclave of this rhyodacite, which in this case is still genetically related to the granodiorite. Similarly for inclusions (B) and (C), an orthopyroxene-bearing assemblage (reaction 3) could represent any of the following origins: a restite inclusion, a xenolith of associated orthopyroxene-bearing rock (for example, of Mt. Donna Buang Rhyodacite in the Warburton Granodiorite; enclave (C)) an accidental enclave of intruded orthopyroxene-bearing rock or a chill-cumulate (see Vernon, 1983).

By analogy with zoned inclusions, the texturally and mineralogically homogeneous, unzoned enclaves have possibly been formed by a similar diffusion controlled, reaction process. Within the zoned inclusions, the reaction process was "frozen" upon final solidification of the total magma system (that is, neglecting the subsolidus readjustments). But, if this process had continued until the chemical potential gradients across the core-rim contact were eliminated, that is, the diffusion

"front" would have progressed across the core, the final enclave would resemble an ordinary, unzoned enclave. Its composition, mineralogy, and texture would be that of the original reaction zone. In the case of multiply-zoned enclaves, a similar argument holds until only one reaction rim remains. Essentially, unzoned and zoned enclaves of the same size may reflect different chemical potential gradients as well as different rates of diffusion for the various components.

A linear trend for the compositional variation of a suite of granitic rocks plotted on a SiO_2-variation diagram is interpreted by White and Chappell (1977) as a mixing trend. After leaving its course, a magma may clear itself, to some extent, of residual restite material; the resulting compositions for the crystalline rocks defining a mixing line between the melt and the restite material (White and Chappell, 1977). However, since the reaction between a granite magma and an enclave appears to be a diffusion controlled process, a restite enclave need not plot on this mixing line defined by the whole rock compositions. This is illustrated for the Lysterfield Granodiorite on a MgO-SiO_2 diagram in figure 9, where the regression line is calculated for the whole rock compositions only. The compositions for enclaves (E) and (F) do not plot on this line: neither do the two unzoned enclaves which also may represent restite material. Depending on the extent to which the enclave has reacted with

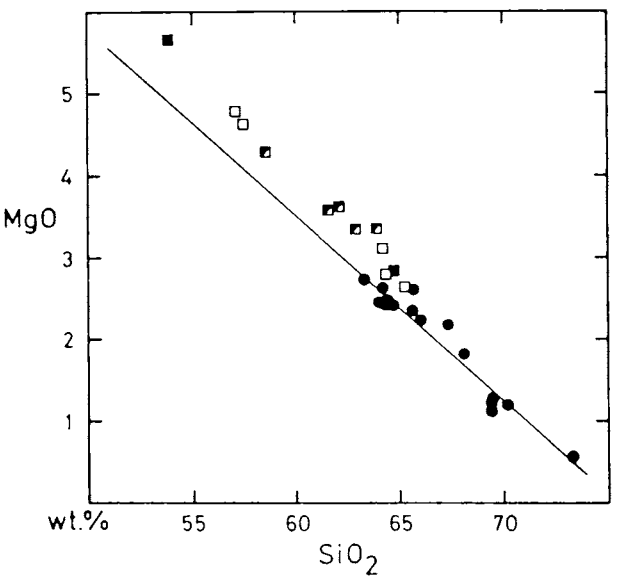

Fig. 9. MgO-SiO_2-variation diagram for the Lysterfield Granodiorite. Circles are whole rock compositions, and squares are restite inclusions (open = inclusion (F); half filled—inclusion (E); filled = others). Regression line is calculated for whole rock compositions only.

the magma, the composition of that enclave will plot closer to the whole-rock mixing line. Furthermore, on a SiO_2 variation diagram, the scatter of compositions of restite inclusions will depend on the choice of the second component. The larger the difference in the flux for the second component relative to the flux for SiO_2, the larger this scatter. If the four enclaves, plotted in figure 9, are representative of the restite material in the magma, their consistent deviation toward high MgO values suggests a relatively homogeneous source for the Lysterfield magma or a crystal fractionation process. Presumably, a more heterogeneous source results in restite inclusions whose compositions show a corresponding scatter on a similar diagram.

ACKNOWLEDGEMENTS

The authors are indebted to Drs. A.J.R. White and R.C. Price of La Trobe University for helpful comments and the use of analytical facilities. Dr. D. Sewell of the University of Melbourne is thanked for aid with the electron microprobe facilities there, while Dr. W. Nesbitt is thanked for numerous useful discussions.

APPENDIX 1

Petrographic descriptions of the samples

Enclave A.—This inclusion is a fine-medium grained diopside-bearing inclusion from the Lysterfield Granodiorite. It measures about 10 × 8 × 4 cm. A mineral foliation is present oriented at right angles to the sample profile. Core (A1) consists dominantly of fine-grained (<1mm) diopside with plagioclase, quartz, and minor sphene. In the center of the core, there is a thin layer consisting of diopside, a carbonate mineral, and coarse-grained quartz. Reaction rim (A2), showing sharp contacts with both the core and the granite (AG), contains medium-grained poikiloblastic hornblende with minor biotite intergrowth, alkali-feldspar, fine-grained plagioclase ($\sim An_{35-40}$), quartz, sphene accessory ilmenite, and needle apatite. Along the contact with the core, biotite in (A2) is very subordinate to hornblende, and across the reaction rim toward the granite contact, the hornblende/biotite ratio decreases, and both minerals become less poikiloblastic. Across the contact between the reaction rim and the granite, the hornblende-biotite ratio changes from about 18.0 to 0.5 for the granite. Shape and symmetry of the inclusion are regular. The width of the reaction rim is always thicker where this rim has developed through the foliation.

Granite (AG) is a medium grained, equigranular granodiorite containing subhedral-euhedral amphibole (hornblende) and biotite with minor sphene, ilmenite, apatite, allanite, and zircon as accessory phases. Plagioclase crystals contain subhedral cores (up to An_{50}) rimmed by oligoclase-albite. The granodiorite is massive and homogeneous in composition. Inclusions (A) and (F) (fig. 6) are from the same locality, where there is an estimated 5 percent of inclusions in the granite.

Enclave B.—This inclusion is a fine-grained anthophyllite-bearing inclusion from the Bulla Adamellite (loc. 7, Bryndzia, ms). It measures about 8 × 6 × 4 cm and has an ovoid shape. Core (B1) consists of interlocking calcic plagioclase (An_{58}) laths with interstitial, equant anthophyllite. The plagioclase is gradually replaced by quartz, whereas the anthophyllite has progressively thicker biotite rims on approaching the outer edge of the core. K-feldspar is rarely present. Intermediate reaction zone (B2) is similar to the core except that only biotite "clots" are retained after anthophyllite and the plagioclase laths

are more replaced by quartz: K-feldspar is common. The outer rim (B3) contains larger equant plagioclase crystals of lower An-content (An_{20-30}) with some corroded relicts of high-An plagioclase. In addition to biotite, almandine (pyrope + spessartine) garnet occurs as euhedral grains within calcic plagioclase, and Fe-rich cordierite occurs as small interstitial grains. K-feldspar is common in the outer rim.

The adamellite (BG) is medium-grained and equigranular, containing euhedral cordierite, subhedral biotite with zircon, apatite, and ilmenite, and some magnetite. Plagioclase crystals contain subhedral cores (up to An_{55}) with rims of oligoclase-albite. Inclusions make up a total of nearly 5 percent by volume in the pluton.

Enclave C.—This inclusion is fine-grained with a biotite-amphibole core and a biotite-only reaction rim (from the Warbuton Granodiorite). Total size is about 40 × 30 × 30 cm. The thickness of the reaction rim is about 8 to 10 cm with sharp contacts with both core and granite. Shape and symmetry are fairly regular. The homogeneous core (C1) has a dominant poikilitic texture with small subhedral crystals of biotite and anhedral Ca-poor clinoamphibole intergrown with laths of plagioclase (labradorite, up to An_{65}), enclosed in coarser-grained, optically continuous quartz and K-feldspar. From the center of the core outward, the amphibole first becomes more strongly twinned, then ragged, intergrown with biotite, and surrounded by quartz. Some large plagioclases, with euhedral cores (up to An_{60}) and rimmed by oligoclase-albite, occur in both the core and the reaction rim. The rim contains less calcic plagioclase (An_{30-40}) altered laths of plagioclase together with quartz, alkali-feldspar, and biotite as the only ferromagnesian silicate. Accessory ilmenite, apatite, and zircon, along with secondary sphene occur in both core and reaction rim. There are isolated patches of fine-grained material within the rim, similar to the core in both composition and texture.

The granodiorite (CG) is fine-to-medium-grained and equigranular. It contains biotite, accessory ilmenite, apatite, and sulfides; sphene is secondary. Plagioclase ($\sim An_{30}$), perthitic alkali-feldspar, and quartz are present in about equal proportions. The granodiorite is homogeneous in composition, as well as massive, with only a few small inclusions.

Enclave D.—This inclusion is a fine-to-medium-grained, amphibole-bearing inclusion from the Tynong Adamellite. It measures about 12 × 10 × 8 cm. It has an asymmetrical position of the core. The contacts between core, reaction rim, and granite are sharp. Core (D1) contains large (up to 3 mm) poikiloblastic, anhedral amphibole, subhedral, fine-grained biotite, and perthitic alkali-feldspar. Plagioclase in the core is rare, whereas ilmenite and apatite occur as accessory phases; there is some secondary epidote. The rim (D2) contains subhedral biotite, medium-grained poikiloblastic amphibole, and large plagioclases. The matrix of the rim consists of abundant fine-grained sodic plagioclase ($\sim An_{25}$), K-feldspar, and quartz. The large plagioclase crystals are up to 2 mm across and are normally zoned with compositions up to An_{45}. The alignment of fine-grained biotite results in a slight foliation in both rim and core trending parallel to the core-rim contact.

Granite (DG) is a coarse-grained, amphibole-bearing biotite adamellite. Phenocrysts of plagioclase and perthitic alkali-feldspar are up to 2 cm in size. The plagioclase phenocrysts have distinct calcic cores ($\sim An_{50}$) and are generally complexly zoned. Biotite occurs as both medium-grained, euhedral crystals and fine-grained subhedral crystals. Amphibole occurs as distinct subhedral crystals enclosed in biotite "clots." Apatite, ilmenite, primary sphene, and zircon comprize the accessory phases. The abundance of inclusions is very low.

Enclave E.—This inclusion is a fine-to-medium-grained amphibole-bearing inclusion from the Lysterfield Granodiorite. It measures about 50 × 35 × 25 cm and has an elliptical shape with an asymmetrical reaction rim varying in thickness from 4 to 12 cm. The contact of the rim with the granite is fairly sharp, whereas the contact with the core is more diffuse. The amphibole/biotite ratio varies from 0.71 in core (E1), through 0.99 in the reaction

rim, to 0.51 in the granite (EG). Amphibole in the core and in the rim occur dominantly as subhedral-to-euhedral sphene and ilmenite. Biotite in the core occurs as subhedral crystals. In the rim biotite is dominantly fine-grained and subhedral, whereas the larger crystals are ragged and appear to be corroded to K-feldspar. Plagioclase in the core is fine-grained with only a few (0.5 cm) large crystals, which are abundant in the rim and in the granite. Distinct cores are present in most large plagioclases, which have compositions of An_{40-45} for the core and An_{15-20} for the rim. Perthitic alkali-feldspar is more abundant in the rim compared with the core. Sphene (both primary and secondary), ilmenite, apatite, and zircon are present as accessory phases in core and rim.

Granite (EG) is a fine-to-medium-grained, equigranular granodiorite containing subhedral-to-euhedral amphibole (hornblende), biotite, and minor sphene, allanite, ilmenite, apatite, and zircon as accessory minerals. Plagioclase occurs dominantly as 3 to 5 mm long phenocrysts which have an average composition of An_{30}. Perthitic alkali-feldspar is mostly interstitial. The granite is homogeneous in composition, as well as massive; inclusions have an estimated abundance of up to 5 percent.

Enclave F.—This inclusion is a fine-to-medium-grained amphibole-bearing inclusion from the Lysterfield Granodiorite. It measures about 50 × 35× 25 cm and has an elliptical shape with an asymmetrical reaction rim varying in thickness from 1 to 8 cm. Core (F1) and the reaction rim have a more diffuse contact than the rim-granite contact. The amphibole/biotite ratio varies from 1.65 in the core, through 0.75 in the rim, to 0.65 in the granite (FG). Amphibole (hornblende) in the core is present as subhedral to euhedral crystals and in clusters of anhedral crystals with biotite, whereas individual biotite crystals are bigger. The textural relationships of all minerals in the rim are similar to that in the granite. The rim contains distinctly more plagioclase compared with the core. Complexly zoned plagioclase occurs both as a groundmass constituent as well as large crystals up to 7 mm long in both inclusion and granite. These large crystals generally have distinct cores ($\sim An_{40-50}$) rimmed by oligoclase-albite. Alkali-feldspar is mostly interstitial and subordinate. Sphene (primary and secondary), ilmenite, apatite, and some sulfide are present as accessory phases in the inclusion.

Granite (FG) is the same as for inclusion (A).

References

Bateman, P. C., Clark, L. D., Huber, N. K., Moore, J. G., and Rinehart, C. D., 1963, The Sierra Nevada Batholith—a synthesis of recent work across the central part: U.S. Geol. Survey Prof. Paper 414-D, p. 1–45.

Borom, M. P., and Pask, J. A., 1968, Kinetics of dissolution and diffusion of the oxides of iron in sodium disilicate glass: Am. Ceramic Soc. Jour., v. 51, p. 490–498.

Brady, J. B., 1975, Reference frames and diffusion coefficients: Am. Jour. Sci., v. 275, p. 954–983.

Bryndzia, L. T., ms, 1976, The geology and geochemistry of the Bulla Adamellite and its inclusions: B.S. thesis, La Trobe Univ.

Carmichael, D. M., 1969, On the mechanism of prograde metamorphic reactions in quartz-bearing pelitic rocks: Contr. Mineralogy Petrology, v. 20, p. 244–267.

Cramer, J. J., ms, 1979, Geochemical variation of some differentiated granitic magmas east of Melbourne, Victoria; Ph.D. thesis, La Trobe Univ. 221 p.

Deer, W. A., Howie, R. A., and Zussman, J., 1974, An introduction to the rockforming minerals: London, Longman,

Didier, J., 1973, Granites and their enclaves: Amsterdam, Elsevier,

Griffin, T. J., White, A. J. R., and Chappell, B. W., 1978, The Moruya Batholith and geochemical contrasts between the Moruya and Jindabyne Suites: Geol. Soc. Australia Jour., v. 25, p. 235–247.

Grout, F. F., 1937, Criteria of origin of inclusions in plutonic rocks: Geol. Soc. America Bull., v. 48, p. 1521–72.

Hine, R., Williams, I. S., Chappell, B. W., and White, A. J. R., 1978, Contrasts between I- and S-type granitoids of the Kosciusko Batholith: Geol. Soc. Australia Jour., v. 25, p. 219–234.

Korzhinskii, D. S., 1970, Theory of Metasomatic Zoning: Oxford, Clarendon Press, 162 p.
Pabst, A., 1928, Observations on inclusions in the granitic rocks of the Sierra Nevada: Univ. Calif. Pub. Geol. Sci, v. 17, p. 325–386.
Reynolds, D. L., 1946, The sequence of geochemical changes leading to granitization: Geol. Soc. London Quart. Jour. v. 102, p. 389-446.
Thompson, J. G., 1957, The graphical analysis of mineral assemblages in pelitic schists: Am. Mineralogist, v. 42, p. 842-858.
Vidale, R. J., 1969, Metasomatism in a chemical gradient and formation of calcsilicated bands: Am. Jour. Sci., v. 267, p. 857–8874.
Vernon, R. H., 1983, Restite, xenoliths and microgranitoid enclaves in granites: Royal Soc. New South Wales Jour. and Proc., v. 116, p. 77–103.
White, A. J. R., and Chappell, B. W., 1977, Ultrametamorphism and granitoid genesis: Tectonophysics, v. 43, p. 7–22.